Acta Biomed 2023; Vol. 94, N. 3: e2023177 DOI: 10.23750/abm.v94i3.14714

Review

Radiological manifestation of avascular necrosis (AVN) in sickle cell disease (SCD): a review of diagnostic imaging

Elsaid Mohamed Aziz Bedair[1], Nasser Jasem Almaslamani[1], Mohamed Yassin[2]

[1]Radiology Department Al Khor Hospital, Hamad Medical Center (HMC), Doha, Qatar; [2]National Center for Cancer Care and Research, Hamad Medical Center (HMC), Doha Qatar

Abstract. Symptomatic avascular necrosis (AVN) imposes a higher risk for acute care consumption in adults living with SCD. Symptomatic AVN, have higher rates of visits to the emergency department, higher rates of admissions, and longer lengths of stay in hospitals. Properly timed diagnosis and early interventions can reduce morbidity and enhance the quality of life in these patients. Vaso-occlusion secondary to sickling leads to osteonecrosis of the joint/bone (AVN, dactylitis) and invites infection (osteomyelitis and septic arthritis). Understanding and awareness of the imaging features related to this major morbidity complication are essential for early diagnosis and prompt management. In about half of the patients with SCD, AVN can lead to chronic pain, particularly in the head of the femur and humerus. Humeral and femoral head AVN tend to be linked with each other. Vertebral bone compression and collapse secondary to AVN have also been reported. The diagnosis of AVN must be accurate, as the condition is complex requiring specific treatment according to the grade of bone and joint involvement. There are several classifications or staging systems used for grading bone and joint involvement. Knowledge of the image patterns and grade of affection in different joints and bones and the degree of progression of AVN lesions can markedly improve management decisions on AVN-specific surgical versus non-surgical interventions and improve patient outcomes. The aim of this report is to summarize the different imaging techniques and their role in the proper/early diagnosis and follow up of patients with AVN with detailed examples of the common sites involved. (www.actabiomedica.it)

Key words: Sickle cell disease, avascular necrosis (AVN), imaging, bones, joints, classification

Introduction

Sickle cell disease (SCD) is a genetic red cell disease that affects the shape of red blood cells (RBC). Sickle hemoglobin (HbS) polymerizes upon deoxygenation, resulting in sickling of RBC. Major clinical manifestations of SCD include hemolytic anemia and vaso-occlusive phenomena resulting in ischemic tissue injury and organ damage. Chronic sequelae of the anemia and vaso-occlusive processes involving the musculoskeletal system include complications related to extramedullary hematopoiesis, osteonecrosis, myonecrosis, and osteomyelitis. Alertness and awareness about the imaging features of SCD complications are critical for timely diagnosis and swift management. Musculoskeletal complications of SCD are common and are often the main causes of their acute and chronic morbidities. Acute manifestations include bony infarcts with vaso-occlusive crises and osteomyelitis, while osteoporosis and osteonecrosis are chronic problems (1,2).

AVN can be asymptomatic in SCD patients for a long time. The natural history of asymptomatic osteonecrosis of the femoral head in patients with SCD is progression to collapse. Early identification of AVN would help in screening and placement of appropriate measures to prevent osteonecrosis in high-risk patients. This is very important because most patients

with osteonecrosis present very late when the only treatment option is total hip replacement with its attendant unsatisfactory results in this group of patients. (3-7) Moreover, in patients with SCD, the radiological manifestations of AVN may be intriguing as it can be mixed and mingled with those for bone infections and bone marrow hyperplasia (8,9). Recognizing the appearance of osteonecrosis, which reflects the underlying pathology, improves clinical-radiologic assessment and is important to guide optimal patient management.

In this updated manuscript the authors tried to review and update knowledge about the different radiological appearance using different imaging techniques (in the past 30 years) that help to investigate and grade the severity of AVN lesions in patients with SCD. An algorithm for imaging evaluation of AVN is suggested to facilitate the clinical appraisal of these cases.

Background

Pathology, pathogenesis and classification

Bone infarction is a debilitating and significant complication of SCD, and it may occur anywhere in the skeleton. It results directly from the sickling of red blood cells in the bone marrow, which causes stasis of blood and sequestration of cells, Ischemia and tissue hypoxia are the consequences and, in turn, worsen the sickling process. The eventual result is cell death. Infarcts typically occur in the medullary cavities and in the epiphysis. They occur in a subchondral location. most common in the femoral head, likely a result of increased mechanical pressure related to weight bearing and often are the source of painful bone crises and can result in greater morbidity owing to its effect on the adjacent joint although they also may be clinically silent and discovered incidentally at radiography (10). Medullary bone infarcts are far more common than osteomyelitis in patients with sickle cell disease (11) but clinical differentiation can be difficult (12). The consequences of the blood vessel occlusion within the bones lead to the development of osteosclerotic strands, bone marrow edematous changes, bone loss and collapse, reactive neovascularity, and fibrotic changes.

The pathophysiology of AVN in SCD entails during hypoxic conditions (infection, physical exercises, acidosis, cold, and dehydration) Sickle Hb (HbS) polymerizes, leading to initial reversible structural changes. After repeated deformation, the RBC membrane is completely damaged. Following deoxygenation, HbS becomes fragile with marked decreased solubility and elasticity. After the restoration of oxygen tension, these abnormal sickle cells fail to return to normal shape (13,14).

The loss of deformability leads to vascular obstruction and ischemia. The membrane damage diminishes the life span of the RBC causing hemolysis, both intra- and extravascular. The destroyed red cells have an irregular surface that leads to increased adherence to and damage to the vascular endothelium. This process enhances vascular obstruction and provokes inflammatory reactions involving white cells, cytokines, and coagulation proteins. Abnormalities in coagulation, white cells, vascular endothelium, and damage to the membranes of red cells share in the pathophysiology of this disease. Increased leukocyte adherence to endothelium also plays a role in the pathogenesis of vascular occlusion. (13,14). A reduction in subchondral blood supply (secondary to vaso-occlusion) produces a state of hypoxia, causing loss of integrity of cell membranes and necrosis of cells. Osteocytes undergo apoptosis; however, phagocytosis cannot occur. Thus, osteocytes are not replaced. This weakens bone remodeling and leads to osteosclerosis.

Macroscopically this induces subchondral collapse and subsequent joint degeneration. (15,16). Histopathology of osteonecrosis is classified into four stages (Table 1). All four stages might be present simultaneously. At early stages, marrow necrosis occurs, and medullary spaces are replaced by granular, eosinophilic

Table 1. Four stages of histopathologic classification of femoral head osteonecrosis (Ref: 17, 18,19).

Type 1, disappearance of hematopoietic marrow and presence of foam cells (nondiagnostic for bone necrosis)
Type 2, necrosis of the fatty marrow in an eosinophilic reticular pattern and presence of oil cysts
Type 3, complete medullary and trabecular necrosis
Type 4, complete necrosis with dense medullary fibrosis and new bone formation.

necrosis, edema, hemorrhages, fibrous reticulosis, and hematopoietic necrosis, with the progressive extension of focal lesions (2,10). At late stages, the death of 50% of osteocytes occurs (trabecular necrosis, bone loss) with fibrosis (fibrotic changes) and collapse (11,12).

In patients with SCD, the radiological manifestations of AVN may be challenging as it can be mixed and intermingled with the changes of bone infections and associated bone marrow hyperplasia which are serious and common complications caused by SCD. In Bahebeck et al. (20) study 7% of patients with SCD were diagnosed with septic arthritis, and 18% with osteomyelitis. Asplenia, impaired complement activity, and phagocytosis are hypothesized to be important factors that predispose patients with SCD to infection of the bone and joints. In addition, infarcted areas of the medullary bone can be a good medium in which bacteria can grow, as reduced blood flow in these regions can result in locally impaired immunological response. Osteomyelitis usually affects the diaphysis of the long bones, but other bones including vertebrae can be sites of infection (8). Patients with sickle cell anemia have reduced height (21). This is believed to be due to bone marrow hyperplasia (8) and bones are generally shorter due to epiphyseal changes subject to ischemia/infarction and vascular compromise to the growth plate with subsequent premature closure of growth plates.

Review

There are many radiological grading and staging classifications for quantifying the extent of AVN involvement in the bone and joint mainly used for AVN of the femoral head. The most used is the Mitchell classification of AVNs (22,23) which is based on MRI signal characteristics within the center of the lesion on T1 and T2-weighted images. The lesion is classified into four stages with stage A representing early disease and stage D representing late disease (Table 2), however, the signal intensity of more than one stage can be found in a single lesion (Figures 1-7).

Second classification is Steinberg staging (24) of femoral head avascular necrosis (Table 3) and quantification of involvement extend is necessary for stages I to V (Table 4), which is the commonly used system similar to the Ficat and Arlet staging and the Association Research Circulation Osseous classification (ARCO) (25-29) which are more simple but with no precise prognostic outcomes, while the Steinberg staging is more concise and delineates the progression and extent of AVN involvement more accurately, it is based on the radiographic appearance and location of the lesion. It primarily differs from the other systems by quantifying the involvement of femoral head changes which allows direct comparison between series. Seven stages of involvement are identified. Following staging, the extent of involvement of the femoral head is recorded as mild, moderate, or severe. This staging system has achieved much recognition by the orthopedic community. Plain radiographs, CT, and MRI can be used in staging and are positive from stage II Steinberg or Ficat classifications while the early stages are essentially categorized by MRI.

The degree of progression of AVN is variable from one patient to another and several factors are influencing the progression, the amount of Hbs, frequency, and severity of associated infective changes, exposure to trauma, and general life still with more physical stresses all are affecting the progress of the AVN and patients with high physical stresses should be handled carefully and bony crises should be evaluated well and followed up frequently as the progression of AVN, especially of the hips can be rapid in these patients (Figure 16) (25,30). Imaging modalities used to diagnose and quantify the degree of affection (grading) and differentiate AVN from other pathologies associated with SCD include mainly conventional plain radiographs, MRI, CT, US, and isotope studies. Each of these modalities had its advantages and limitations.

Table 2. Stages of chronological activity of AVN according to Mitchell classification of avascular necrosis showing the different T1-w and T2-w characteristic signal according to tissue present in osteonecrosis area (Ref: 22).

Stage A: T1 Hyperintense, T2 Intermediate, Signal analogous to that of fat (Hyper acute)
Stage B: T1 Hyperintense, T2 Hyperintense, Signal analogous to that of subacute blood (acute)
Stage C: T1 Hypointense, T2 Hyperintense, Signal analogous to that of fluid/edema (chronic)
Stage D: T1 Hypointense, T2 Hypointense, Signal analogous to that of fibrosis (late chronic)

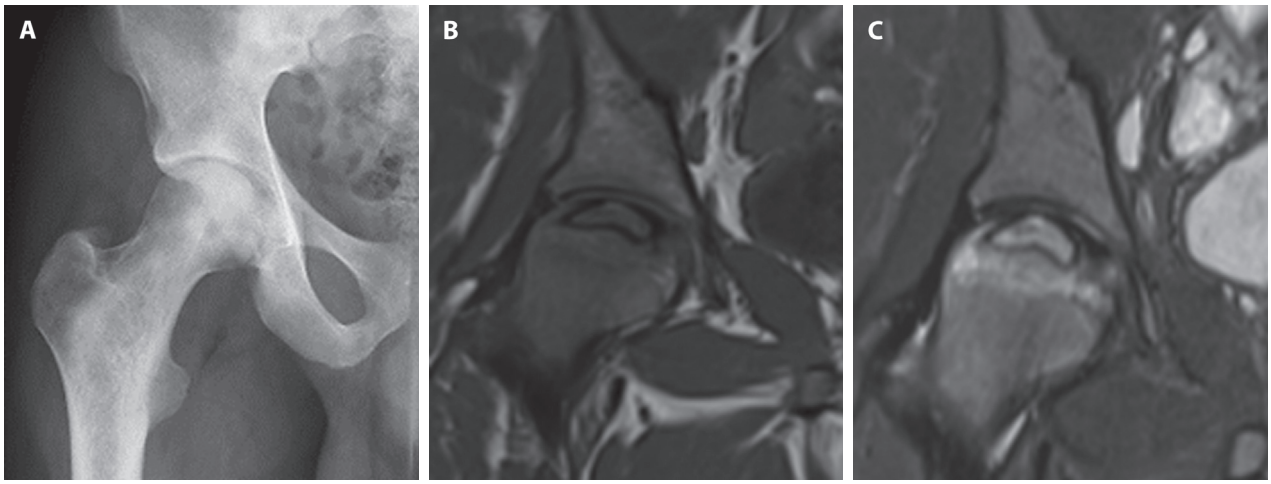

Figure 1. Plain Xray Rt hip AP (A) views for patients with severe pain in Rt hip show only very subtle density changes in the femoral head no subchondral lucent (crescent) line could be identified while (B) and (C) are MRI T1 and T2 with fat suppression for the same hip showing subchondral hypointense crescent line around a small area of relative T2 hyperintensity and T1 intermediate to low signal intensity representing stage c AVN (Mitchell's MRI staging classification) and stage II Steinberg (stage II Ficat) classification by plain radiography while the staging is upgraded by MRI to Stage IIIc according to Steinberg classification and still stage II Ficat classification, this is an example of the MRI merits over plain radiography in diagnosis and staging of early bone necrosis and highlighting the advantage of Steinberg in the quantification of the femoral head involvement over Ficat classification.

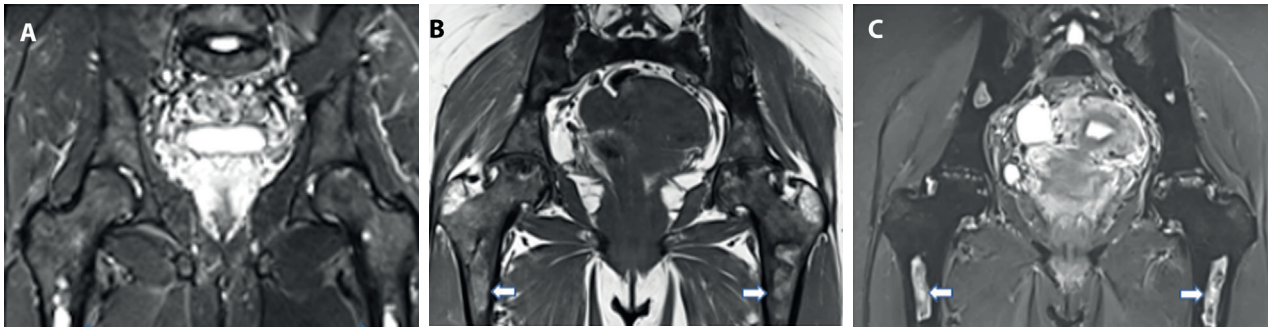

Figure 2. A T2 fat suppressed coronal sequence for the pelvis and upper thighs demonstrating elongated hyperintense medullary lesion within the upper shaft of both femora (arrows) denoting early bone marrow necrosis with marrow edema stage A/B Mitchell classification, note the AVN changes within both femoral heads, (B)T1 coronal without fat suppression and (C)T2 tirm coronal with fat suppression for pelvis and upper thighs after one year showing the same areas of osteonecrosis within the bone marrow of upper femora but with variable degrees of chronic changes appearing as bizarre areas of irregular mosaic hypo and hyperintensity in both T1 and T2 sequences representing areas of necrosis fibrosis and marrow edema with relatively more hyperintense appearance in T2 and relative hypointense appearance in T1 which denote mixed stages B,C and D (mainly C) Mitchell classification, together with variable degrees of AVN and irregular collapse of both femoral heads about stage Vc-VI according to Steinberg classification (Ficat IV).

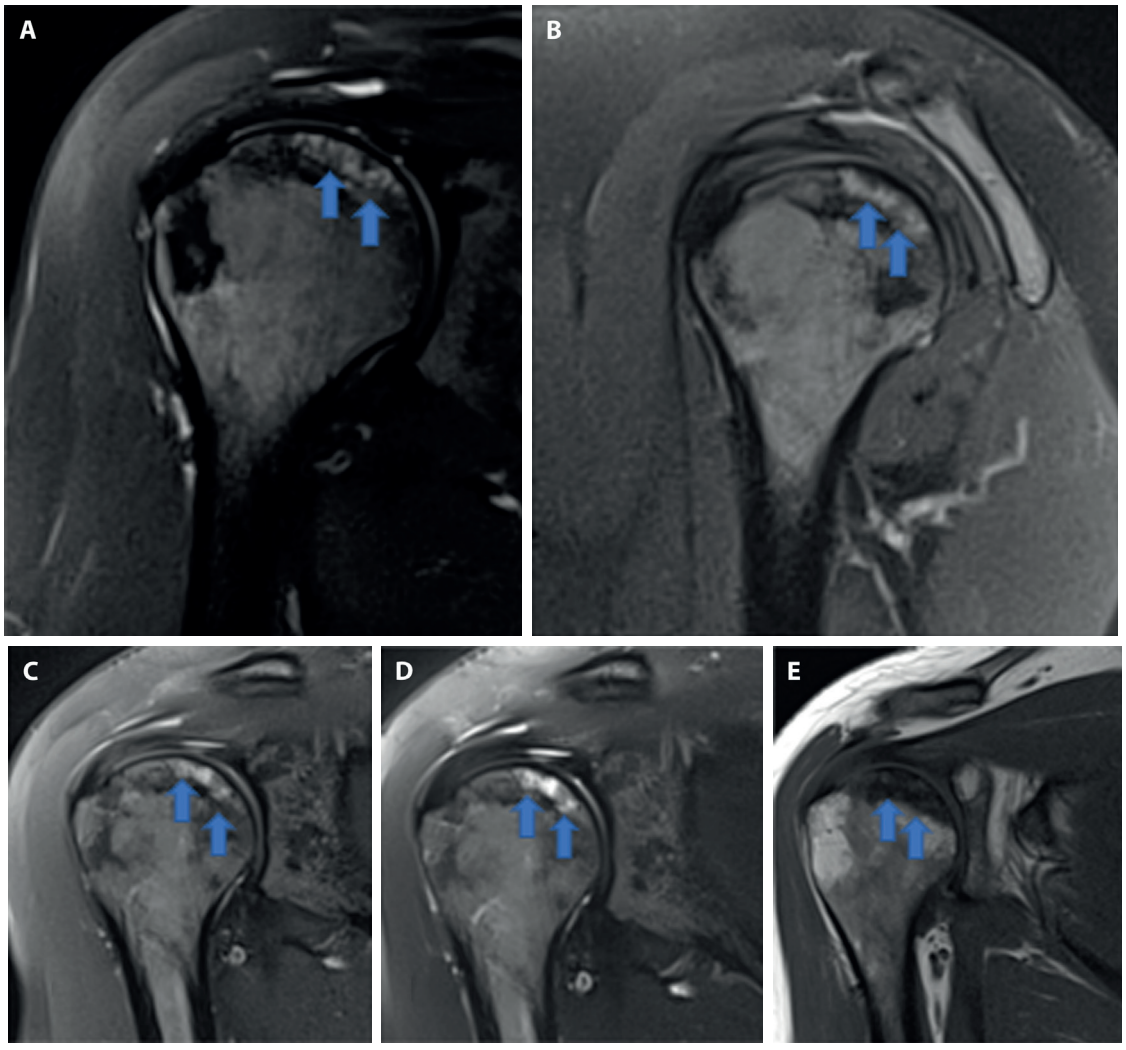

Figure 3. Rt shoulder (A) T2 blade fs coronal and (B) T1 fat sat coronal showing subarticular band-like areas of hyperintense T1 and T2 appearance involving about 30% of the humeral head with no associated humoral head collapse or flattening appearance is that of AVN stage II Ficat/stage IIIb Steinberg classification and hyperintense appearance of the central parts of both infarcted areas in T1 and |T2 denoting stage B Mitchell classification, (C) sagittal PD blade FS coronal (D) T2 blade FS and (E) T1 coronal for the same patient but 2 years later demonstrating more increase in the size of the subarticular necrotic area and there is the development of mild irregularity of the articular surface of the humeral head together with the change of the T1 signal to hypo intensity denoting more progression of the AVN from stage IIIb to IVc Steinberg and from II to III Ficat, and according to Mitchell classification it is progressed to stage C.

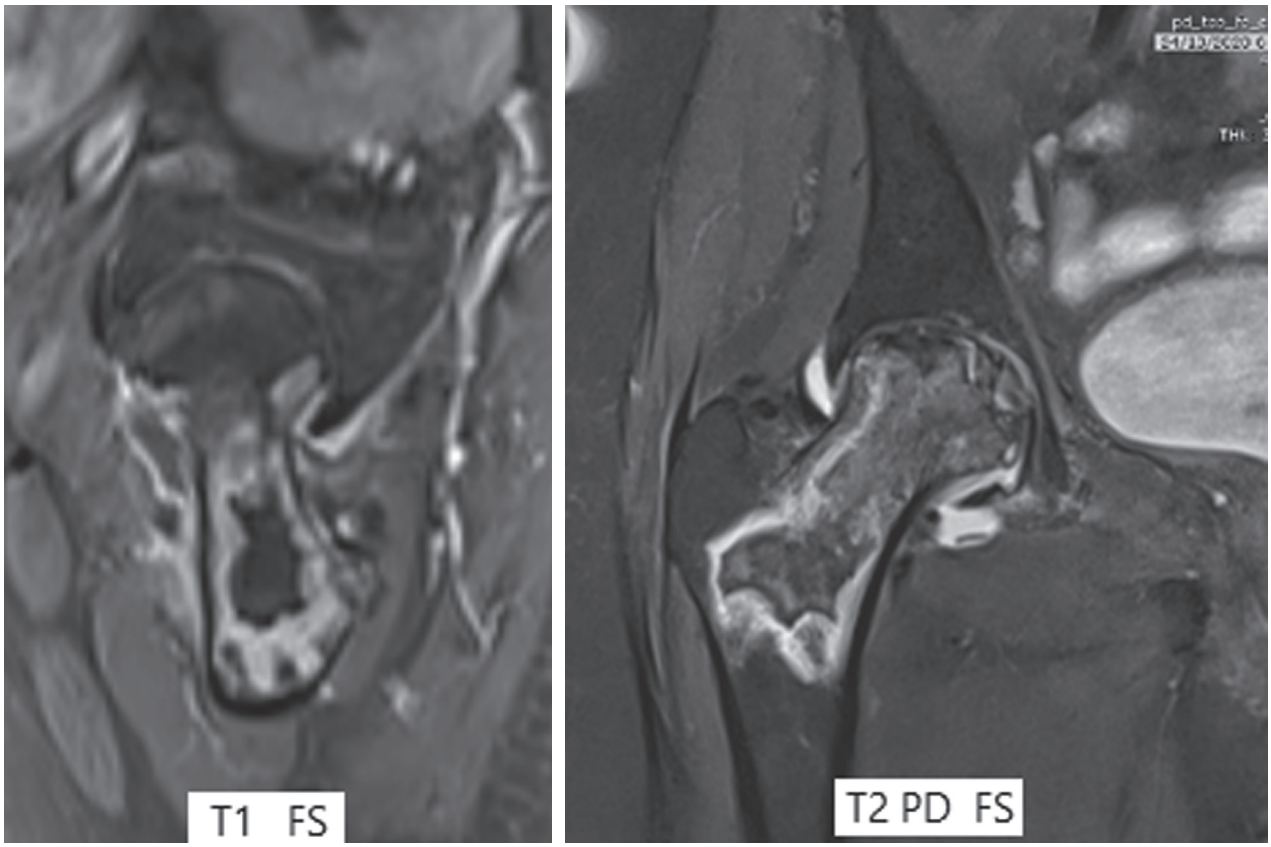

Figure 4. Sagittal T1 FS and coronal T2 PD FS sequence for the Rt hip, and upper femur in a patient with sickle cell anemia showed the serpiginous medullary intermediate and low signal intensity lesion in T2 FS with surrounding markedly hypointense rim and more peripheral hyperintense zone while in T1 the central medullary lesion appears markedly hypointense and the surrounding rim is more hypointense with surrounding zone showed marked hyperintensity, appearance consistent with medullary infarcts representing mixed C and D stages of the central part of the lesion and recent extension of the osteonecrosis around the older one (stage B peripheral part) according to Michell classification for AVN while the markedly hypointense line in-between presenting fibrosclerotic rim separating the relatively recent from the relatively old infarcted areas.

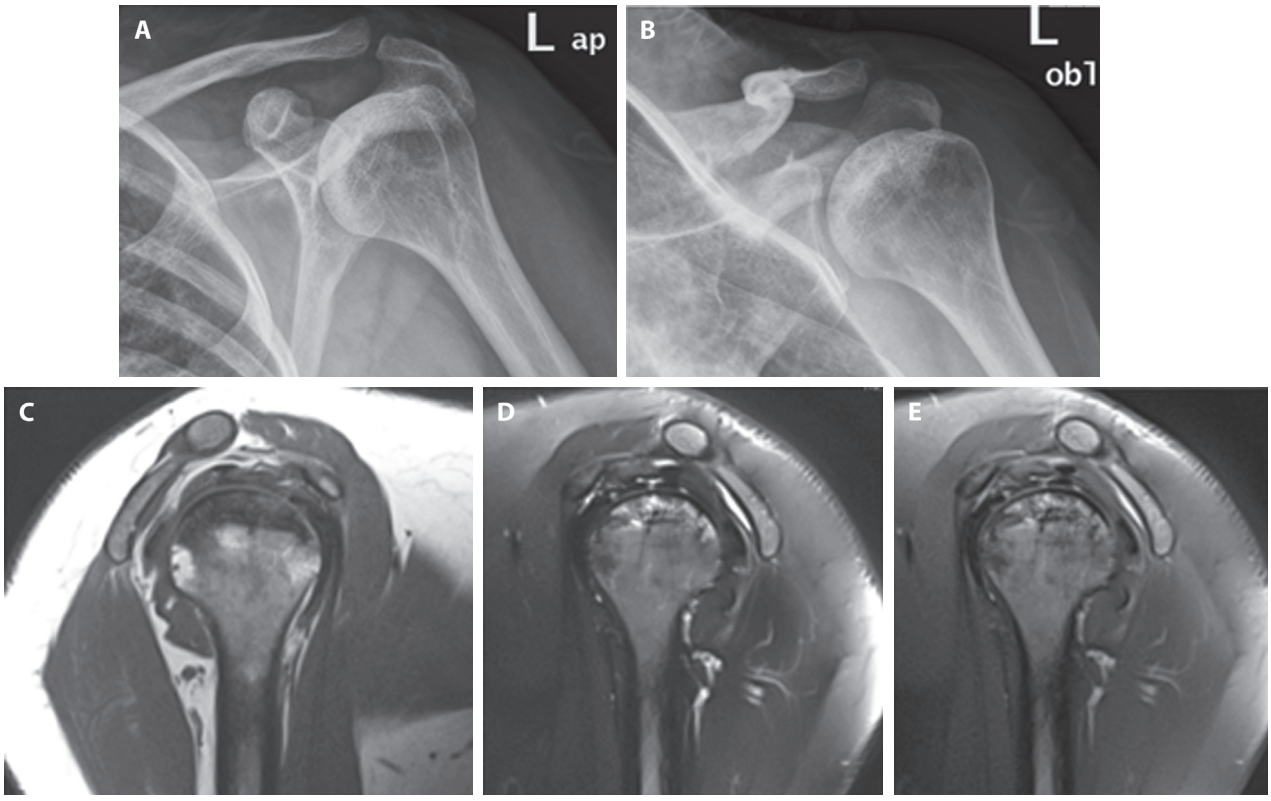

Figure 5. Plain X ray left shoulder AP (A) and lateral oblique (B) as well as MRI (C) T1, (D) T2 blade with fat suppression, (E) PD blade with fat suppression showing heterogeneous density with ill-defined patchy lytic and sclerotic small foci (snowstorm appearance) involving the left humeral head with preserved contour of the articular surfaces, no collapse or crescent sign and no glenoid involvement in plan X rays corresponding to stage Iic Steinberg classification (stage II Ficat) while MRI showed subarticular band of AVN involving more than 30% of the circumference of the humeral head which appear as variable hyperintense in both T2 and PD fat suppressed sequences and hypointense in T1 with no flattening or gross irregularity of the articular bony surfaces appearance is consistent with stage IIIc Steinberg classification, stage II Ficat classification and stage C Mitchell classification (hypointense T1 and hyperintense T2 lesions) so MRI did upgrade the degree of involvement of the humeral head AVN.

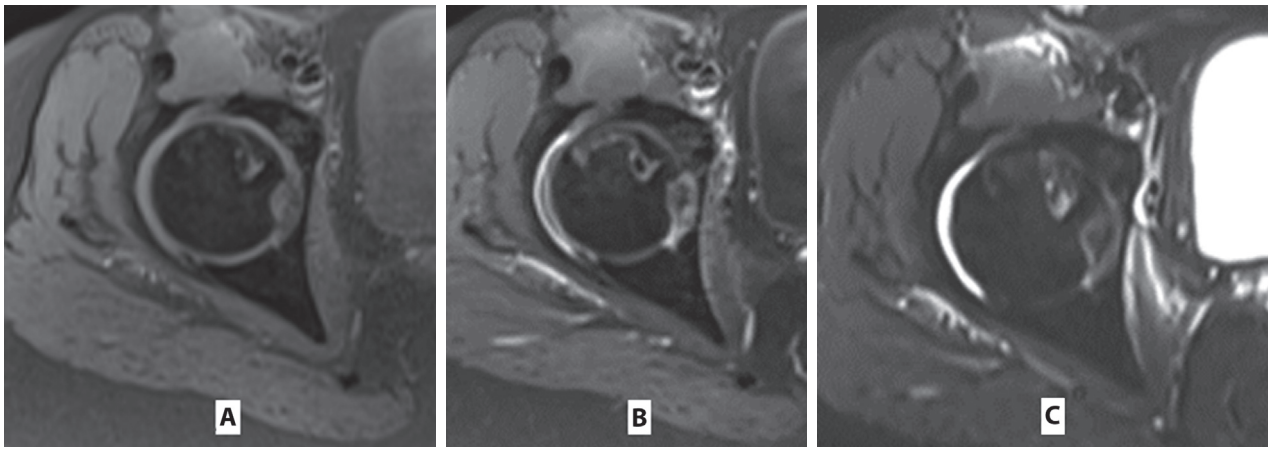

Figure 6. T1 FS precontrast (A), T1 postcontrast (B), and T2 STIR (C) showing small focal hypointense T2 lesion appearing hypointense in T1 with no enhancement and surrounding hyperintense rim in T1 and T2 sequences with no post-contrast enhancement denoting tiny focus of AVN stage D Michell surrounded by another focal area of stage B AVN, there is another linear subarticular lesion showing intermediate to hyperintensity in T2 and is to subtle intermediate intensity in T1 and showed postcontrast enhancement denoting revascularization of subchondral linear AVN stage A Mitchell classification, no subchondral crescent sign and intact articular surface of the femoral head so it is graded as Steinberg stage I B, plain X-ray for this hip was normal.

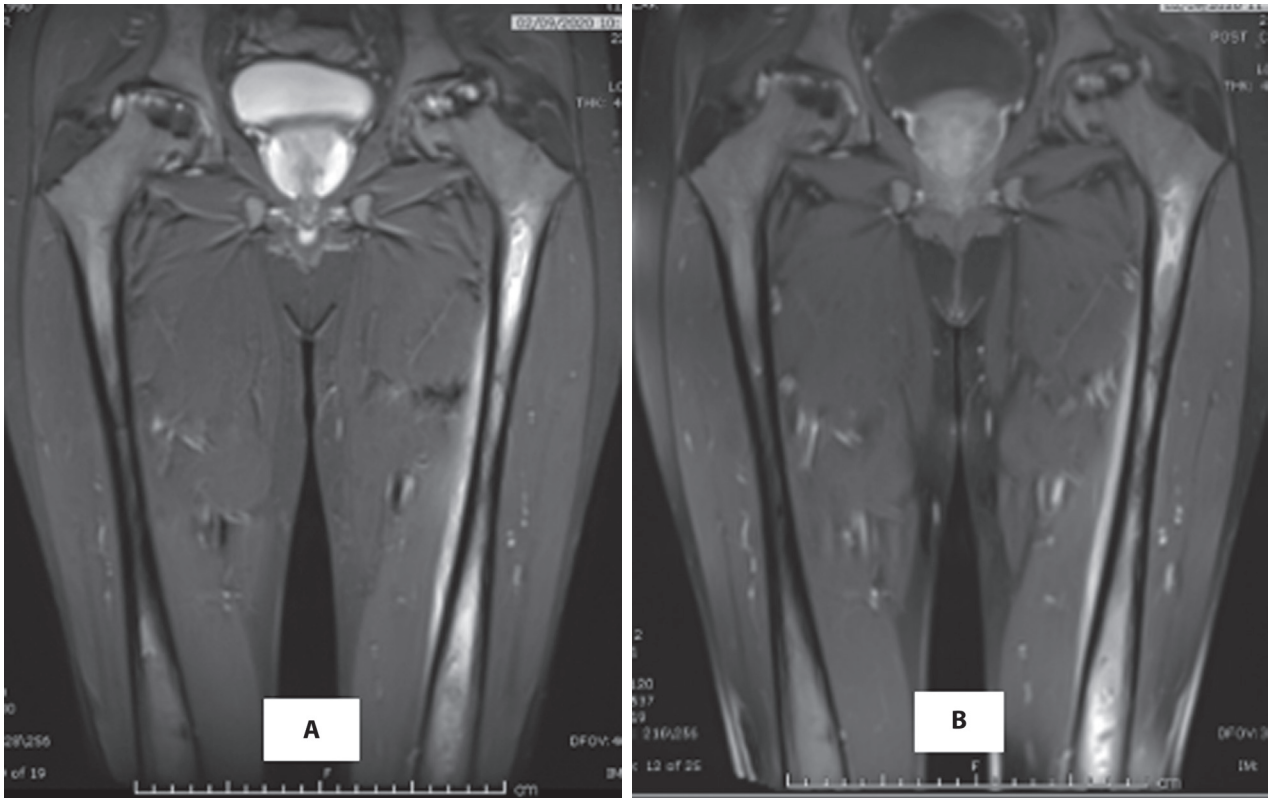

Figure 7. MRI Coronal T2 fat suppressed sequence (A) and T1 post-contrast sequence with fat suppression (B) for both femora showing considerable bone marrow edema involving the medullary cavity of the left femur with associated periosteal reaction and mild edema of the soft tissues around the periosteal reaction and postcontrast enhancement of the same areas in a patient with SCD denoting rather acute osteomyelitis, note associated AVN changes within both femoral heads with different stages of involvement according to Mitchell classification (stage D involvement in Rt femoral head (hypointense T1 and T2) while the left hip showed mixed stage D and stage B (hyperintense T1 and T2) areas.

Table 3. Steinberg staging classification (Ref:24). (Figures 8-15).

Stage 0: normal or non-diagnostic radiographs, MRI and bone scan of at-risk hip (often contralateral hip involved, or patient has risk factors and hip pain).
Stage I: normal radiograph, abnormal bone scan and/or MRI (Figure 6)
Stage II: cystic and sclerotic radiographic changes (Figures 1,5,8)
Stage III: subchondral lucencies or crescent sign (Figures 3,5,9,10,11)
Stage IV: flattening of femoral head, with depression graded into (Figures 3,9,10,12) • mild: <2 mm • moderate: 2-4 mm • severe: >4 mm
Stage V: joint space narrowing with or without acetabular involvement (Figures 2,10,13,14,15)
Stage VI: advanced degenerative changes (Figures 2,13,14)

Table 4. Quantification of the extent of involvement of the joint (Stages I to V).

Stage I and II • A, mild: <15% head involvement as seen on radiograph or MRI • B, moderate: 15% to 30% • C, severe: >30%
Stage III • A, mild: subchondral collapse (crescent) beneath <15% of articular surface • B, moderate: crescent beneath 15% to 30% • C, severe: crescent beneath >30%
Stage IV • A, mild: <15% of surface has collapsed, and depression is <2 mm • B, moderate: 15% to 30% collapsed or 2-4 mm depression • C, severe: >30% collapsed or >4 mm depression • Stage V
A, B or C: average of femoral head involvement, as determined in stage IV, and estimated acetabular involvement.

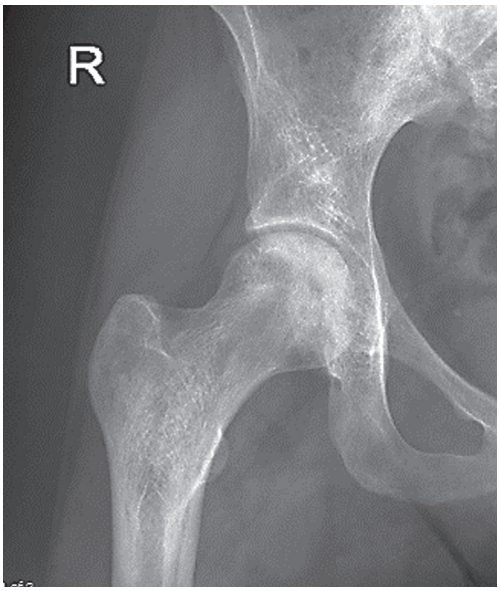

Figure 8. Plain radiograph of the Rt hip AP view showing early patchy sclerosis and lucencies of the right feral head with no collapse or crescent sign (snow storm appearance for femoral head) and associated patchy sclerosis of the hip bone and upper femur consistent with early avascular necrosis stage II Steinberg classification and Ficat classifications. Sclerosis indicates areas of new bone on dead trabeculae. Lucency indicates the resorption of dead marrow and trabecular meshwork.

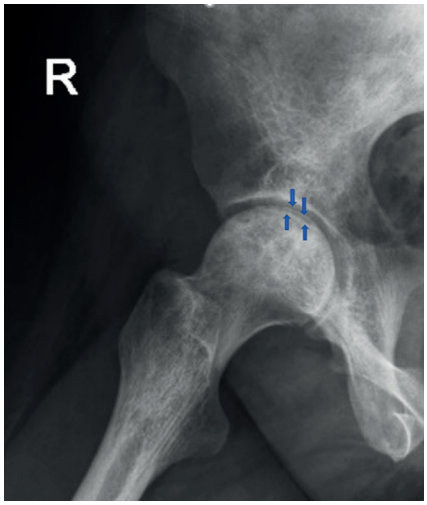

Figure 9. Plain radiograph of the Rt hip lateral oblique view showing early patchy sclerosis of the right feral head with no collapse but there is identifiable subchondral lucent (crescent) line appearance consistent with early avascular necrosis stage IIIa Steinberg classification (stage II Ficat classification).

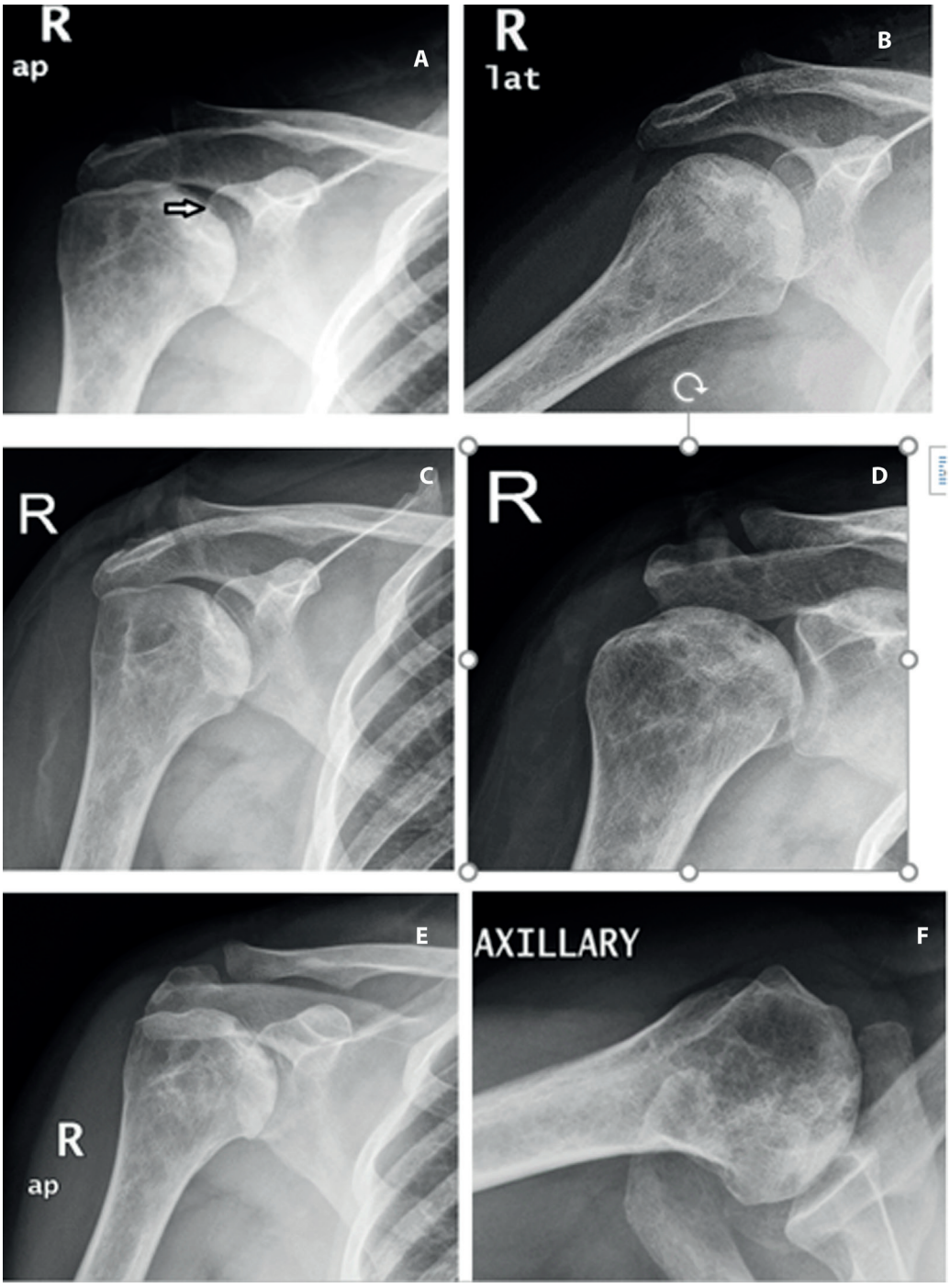

Figure 10. Plain X-ray shoulder AP and lateral views 2017 (A and B) revealed a subarticular lucent line (crescent sign) within the humeral head which revealed AVN Stage IIIa Steinberg classification (Ficat Stage II) with heterogenous patchy sclerosis and lucencies, one year later (2018) AP and lateral radiographs (C and D) showed progression of the AVN to stage IVb Steinberg (stage III Ficat) and another year later(2019) AP and Axial views (E and F) the condition progressed to stage Vc Steinberg classification (only narrowing of joint space and no gross glenoid involvement or gross degenerative OA changes of the shoulder identified (still stage III Ficat), thus stressing the advantage of Steinberg classification in the quantification of the degree of AVN involvement.

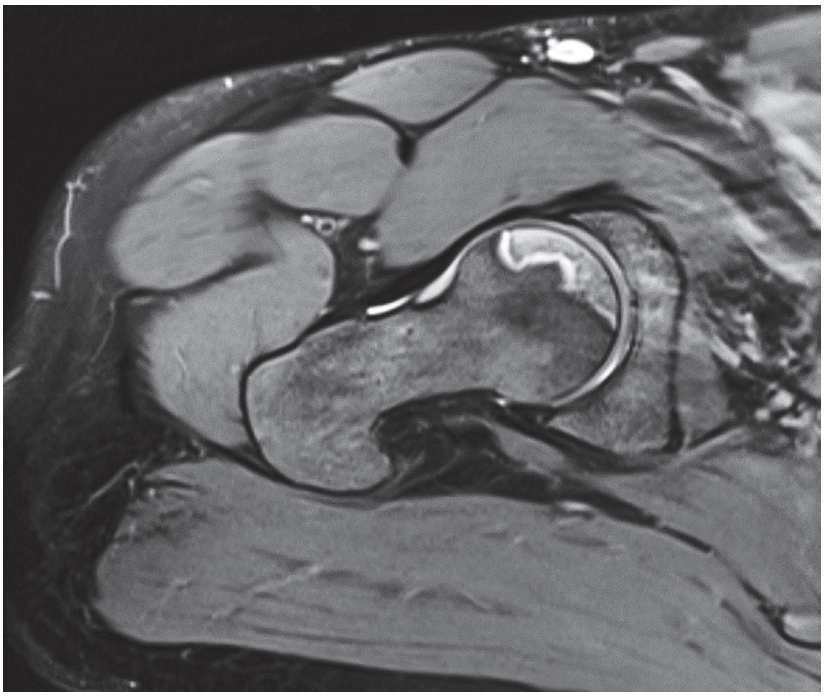

Figure 11. MRI T2 fat suppressed axial sequence showed double line which is composed of a hypointense peripheral border and a hyperintense inner border, staging of the lesion according to Steinberg classification is stage IIIc (Ficat II).

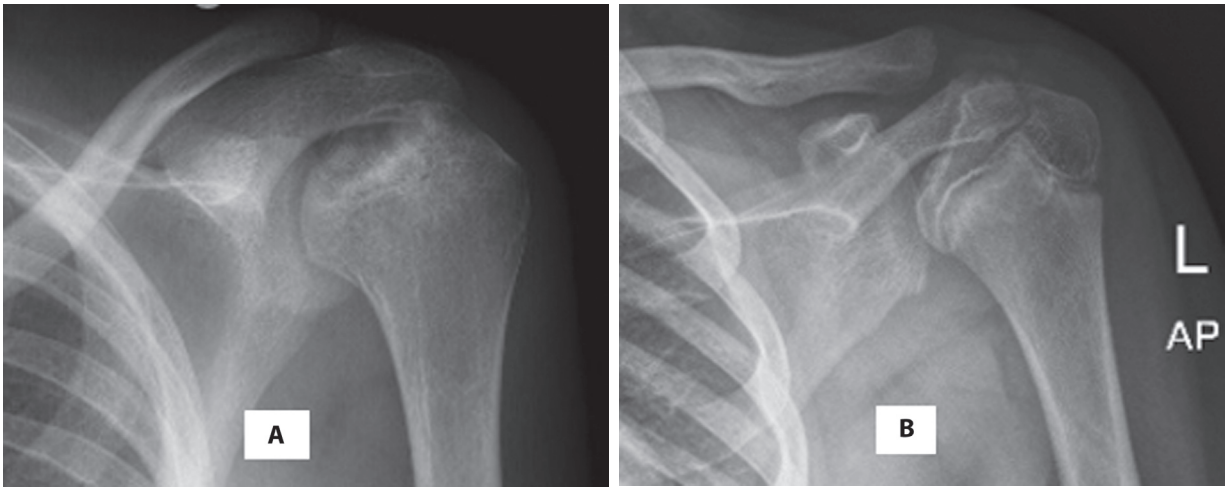

Figure 12. A and B Lt shoulder X-rays for two different patients with SCD (one adult and one before epiphyseal closure) showing destruction flattening and irregular sclerosis involving more than 30% of the humeral heads denoting AVN stage Ivc Steinberg, stage III Ficat classifications.

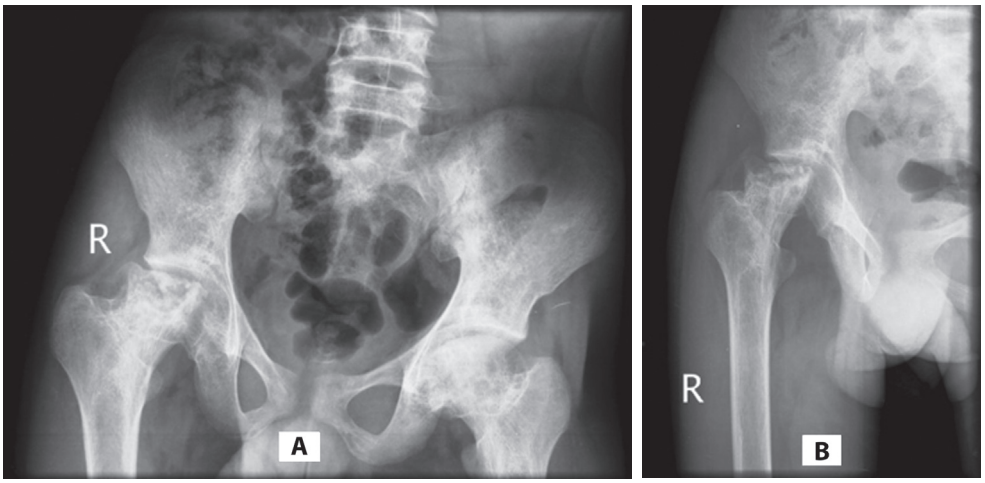

Figure 13. Plain X-ray AP both hips (A) and Rt hip lateral view (B) demonstrating stage IV AVN in both hips according to Ficat classification while according to Sheinberg classification Rt hip showed stage VI AVN with considerable deformity and subluxation of the Rt femoral head and associated acetabular involvement, while the left hip showed stage Vc.

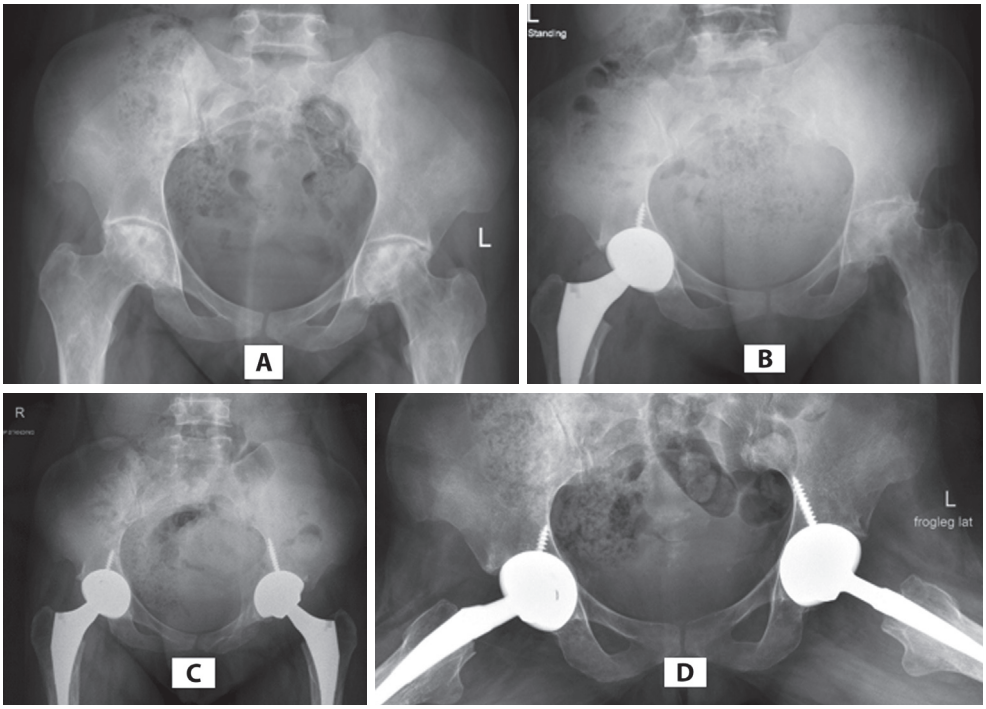

Figure 14. A, B, C, and D : Plain X-ray of both hips AP view (A) (2018) demonstrating irregular contour of the articular surface with deformity and irregular subarticular lytic and sclerotic areas with relative narrowing of the joint space and mild acetabular involvement corresponding to stage Vc to VI Steinberg classification (stage IV Ficat) within both right and lefts hips, (B) three year later (2021) The patient underwent Rt hip total replacement while the left hip showed more progressive course with extensive deformity and development of degenerative OA changes (stage VI Steinberg classification), (C and D, AP and frog leg positions) one year later (2022) total replacement of the Lt hip was performed as the definitive line of treatment for the progressive AVN involvement of the Lt hip.

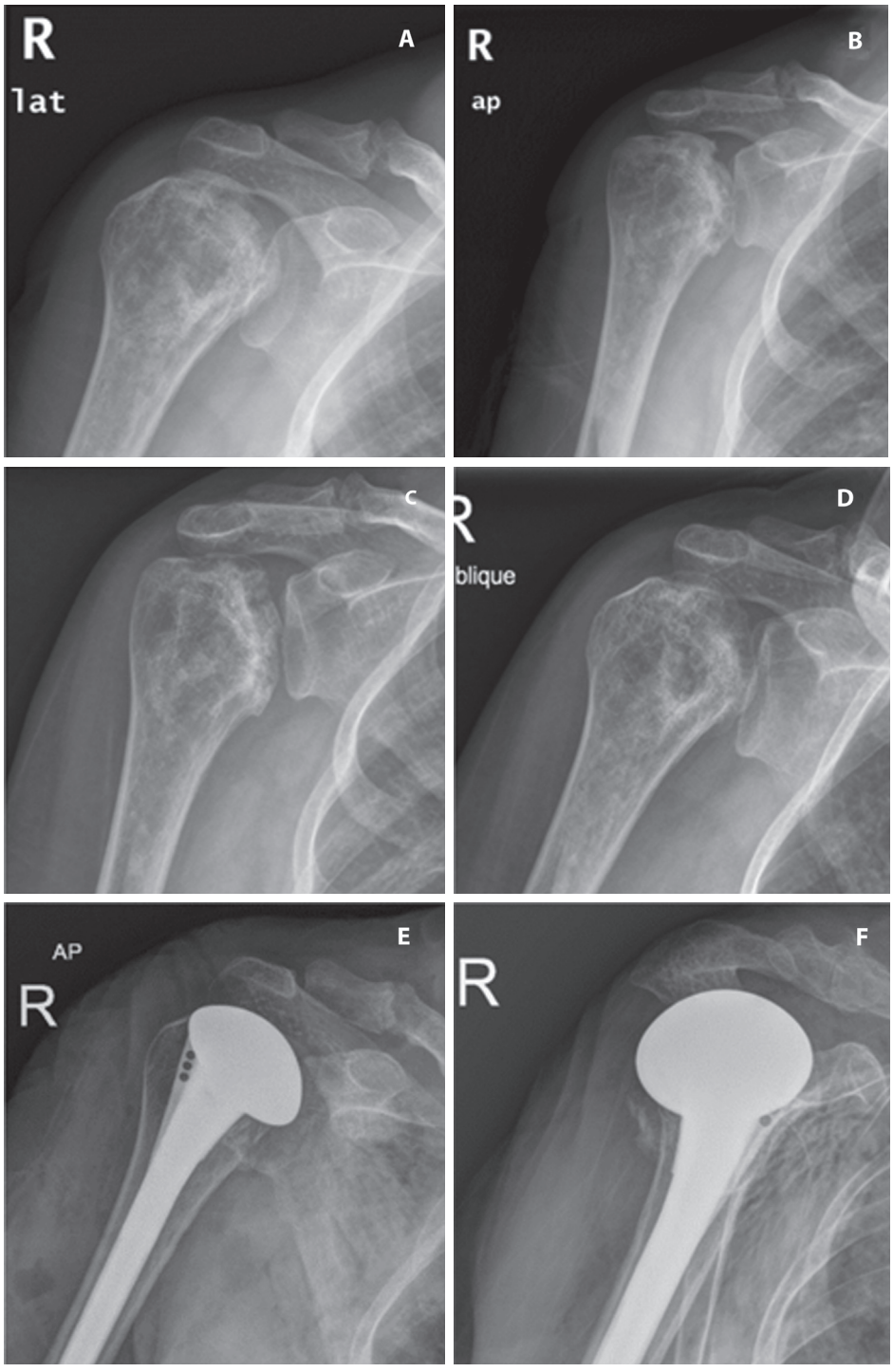

Figure 15. Series of plain X-ray shoulder A&B AP and lateral oblique for Rt shoulder 2017, C and D 2019, and E and F 2021 demonstrating marked deformity, flattening, and irregularity of the head of the right humerus with subarticular sclerosis and cyst-like changes together with intramedullary calcification in the neck of the humerus which are more progressed in 2019 examinations and representing AVN stage Vc Steinberg classification (Ficat IV), and the examination was done in 2021 after shoulder replacement. Note old fracture Rt clavicle with pseudoarthrosis.

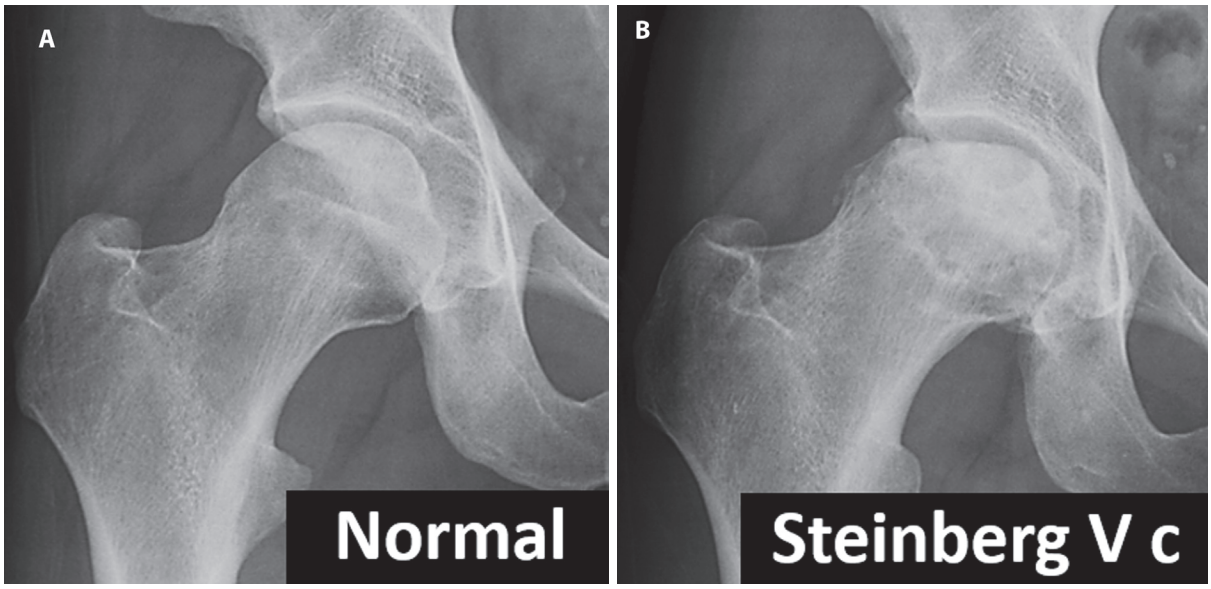

Figure 16. (A) Plain X-ray Rt hip AP views showing a healthy hip joint, in a few months (B) osteonecrosis has progressed to collapse flattening and fragmentation of the femoral head Stage IV Ficat classification and stage Vc Steinberg classification.

a. Conventional plain radiography

It is the most frequently accessible modality at a lower cost. This modality does not identify the early acute bony changes (like bone marrow edema) that occur in osteonecrosis. However, it is a good modality for following the progression of osteonecrosis. With time, the infarcted areas develop centrally lucent and peripherally sclerotic areas with serpiginous wavy margins forming patchy heterogenous lucencies within the involved metaphysis, diaphysis, and epiphysis (Figures 1,8,9,10,16). This is followed by the appearance of subchondral/subarticular lucent lines signifying the border of the infarcted area (crescent sign) that can be identified by good quality plain X-rays (Figures 9,10). Later, chronic changes can be identified as patchy bony sclerosis and linear osteosclerotic strands parallel to the cortical margin (these can lead to a "bone within bone" appearance) (8). Eventually, the progression of AVN leads to subarticular bone resorption with subsequent depression of the articular surfaces, collapse, and fragmentation of the region (Figures 10,12).

These pathological changes cause degenerative osteoarthritic changes and deformities of the affected joint which are well recognized by conventional radiographs (Figures 13,14).

Therefore, conventional plain radiography has no rule in the early detection of AVN but is good for follow-up of AVN evolution, for evaluation of post-interventional therapeutic effects, for the staging of AVN (Figures 10,12,14,15,16,17) and for documentation of late chronic bony changes and deformities (Figure 13). These chronic consequences often necessitate joint replacement (Figure 14,15). During the acute bone crisis in SCD patients, the main and difficult encounter is to differentiate clinically and radiologically between the medullary bone infarcts (more common) from osteomyelitis (31,32), as the initial radiographs are usually normal in the early development of both infarctions and infection (33) Later bone infarction can be diagnosed in films that display patchy latencies, sometimes with periosteal reaction and later by the appearance of bony sclerosis and or collapse (Figures 6, 16) (13). Associated osteomyelitis can be diagnosed by the appearance of periosteal reaction sequestrated bone fragments, involucrum, and cloaca appearance as well as associated soft tissue swelling and later by the occurrence of irregular bony sclerosis.

Other modalities such as ultrasonography (US), MRI (Figures 7,18), and isotope scanning are more informative in the differentiation between acute bone infarction from acute osteomyelitis. **(31,32)**

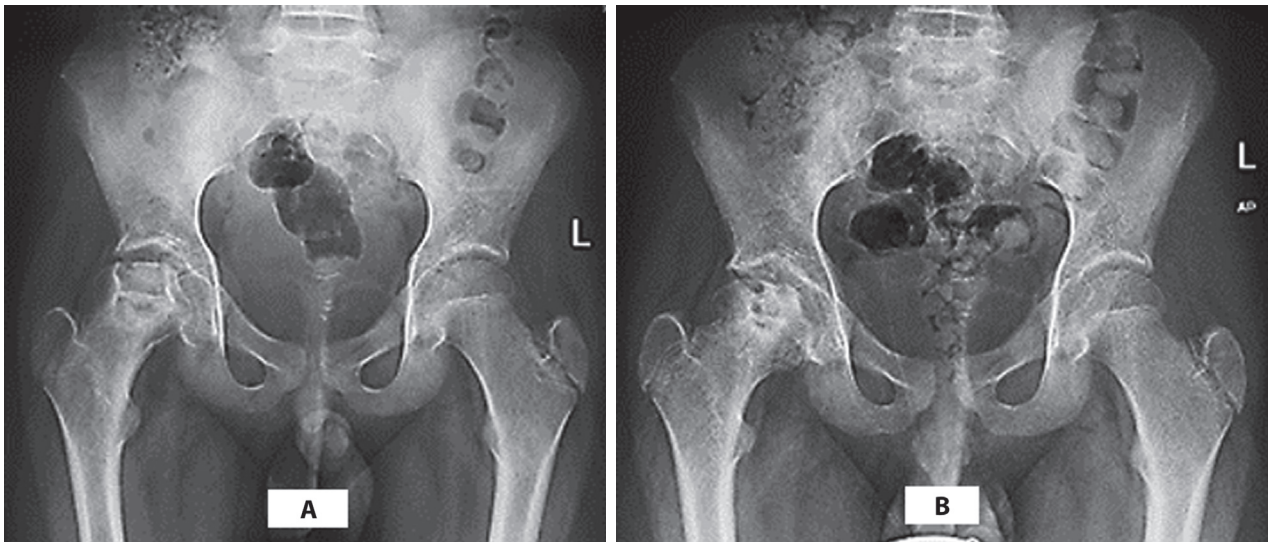

Figure 17. AP both hips A and follow up 6 months B after drill therapy showing AVN Involvement of the immature Rt femoral head epiphysis resulted in partial flattening and collapse of Rt femoral head, epiphysial-metaphyseal overlap, a wide relatively short Rt femoral neck (A) and mild mushroom deformity of the more mature femoral head with residual drill holes identified and the degree of head collapse decreased (relative re-expansion) in follow up exam (B), the articular surface and joint space are generally preserved and little or no disability resulted.

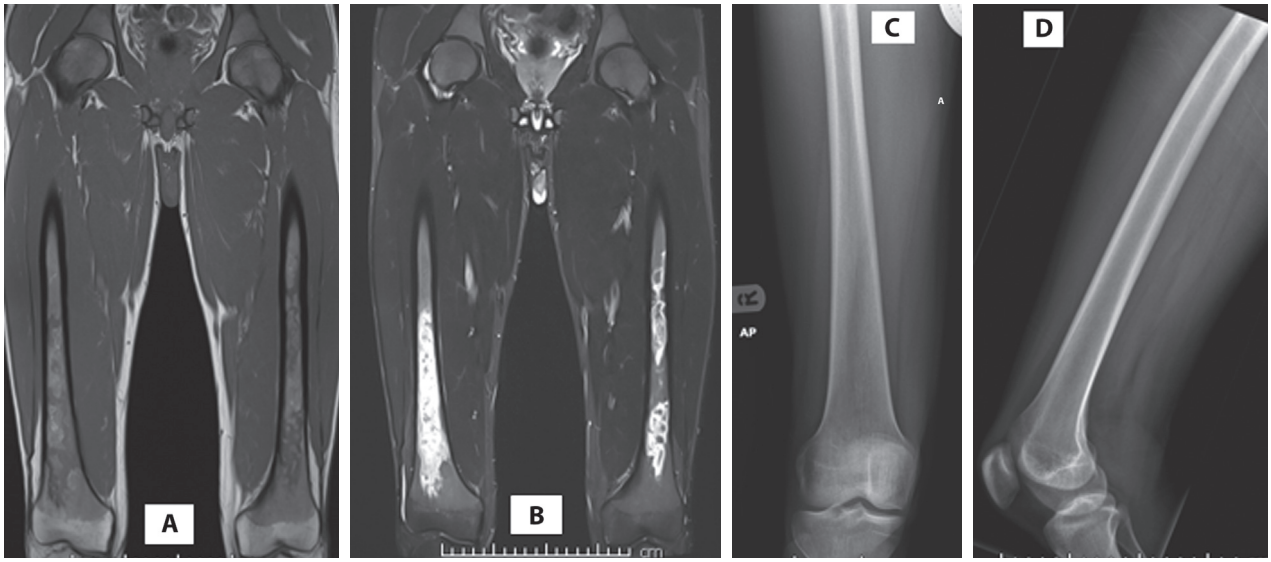

Figure 18. Patient with sickle cell anemia complaining of pain in the lower thighs, A coronal T1 sequence without fat suppression for both thighs and knees demonstrating elongated mixed heterogenous serpiginous outlined hyper and intermediate signal intensity within the medullary cavities of middle and lower thirds both femora with intact cortex while in (B) Coronal T2 sequence with fat suppression the same areas appear heterogenous markedly hyperintense denoting early bone marrow necrosis and edema, no periosteal fluid or soft tissue involvement around the bones (no signs of osteomyelitis), C and D are Plain X ray both thighs and knees AP and lateral views demonstrating no obvious bony abnormality within the med and lower femora, according to plain X ray there are no signs of AVN while according to MRI there are AVN lesions stage B Michell classification of AVN, example illustrative for the advantage of MRI over plain X ray in identification of acute osteonecrosis of medullary cavities of long bones.

b. MRI

It is the modality of choice in the evaluation of AVN it plays a crucial role in the early detection and staging of osteonecrosis; it allows clear quantification, staging; and evaluation of lesions that are undetectable on plain radiographs with excellent anatomical depiction, it is very valuable in follow up with no radiation hazards.

MRI can be useful for illustrating infarction which manifests as edema with increased T2 signal in the acute phase (Figures 6,9,18) and as a fibrotic and sclerotic pattern with low signal on all sequences in the chronic phase (Figures 4,7). The T2 weighted images, specifically, illustrate areas of increased signal intensity because of bone marrow edema. Initially, the signal in the center of the infarction usually resembles that of normal marrow, and acutely (6), an ill-defined area of the high signal may be present (Figure 18), and the peripheral borders may enhance in post-contrast sequences. Over time, a low T1 serpiginous rim develops. A double line which is composed of a hypointense peripheral border and a hyperintense inner border is often visible on the T2 weighted image (Figure 11). This centrally increased T2 signal represents granulation tissues surrounded by dark lines representing the sclerotic bone with chronicity of the lesions the heterogenous appearance of the area of necrosis increases with increased fibrosis and bony sclerosis which appear hypointense in both T1 and T2 sequences (Figures 7, 4).

MRI can be a useful tool in the differentiation of osteonecrosis from osteomyelitis but with some limitations, important MRI differentiating points of osteomyelitis from osteonecrosis of long bones include extensive marrow edema with associated serpiginous and tubular marrow enhancement in metaphysis/diaphysis with extensive associated periosteal reaction/subperiosteal collection (Figure 7) and adjacent soft tissue swelling and edema while the diffuse low signal of the vertebral bodies and medullary cavities of long bones in MRI examinations are consistent with hyperplastic hematopoietic red marrow and in some cases associated hemosiderin/iron deposition replacing the normal bright fatty marrow, especially in the vertebrae (13,31,33,34).

The disadvantage of MRI modality includes limited availability, rather high cost, sometimes requiring anesthesia (in claustrophobic patients and young children) as well as the potential hazards of MR contrast.

c. CT examination

It offers a respectable anatomical description of the lesions and can detect very small changes, and visualize areas invisible to plain radiography, in addition, it is more valuable in the quantifications and staging of the bony involvement (35). Its accuracy is equivalent to that of MRI even though some authors found that CT identifies subchondral fractures and femoral head collapse better than MR imaging (Figure 13). High-resolution CT is a valuable tool for precise grading of the degree of involvement of the femoral head (36). CT is also valuable in the evaluation of spinal involvement (Figure 19).

A meta-analysis provided strong evidence of the high diagnostic efficacy of single photon emission computed tomography/computed tomography (SPECT/CT) in patients with avascular necrosis (AVN) of the femoral head (37). However, the disadvantages of using CT modality is mainly due to the considerably higher dose of radiation hazards so it is not suitable for a follow-up examination and it is still more expensive and less available compared to conventional radiographs (38).

d. Ultrasonography (US)

It can be a useful modality in differentiating osteonecrosis from osteomyelitis and septic arthritis from AVN, It has the advantage of being quick, portable, noninvasive, and more acceptable to children.

The high-resolution US allows the characterization of soft-tissue changes, (soft tissue induration, fat necrosis, and hematoma), fluid collections, periosteal elevation, and subperiosteal collection can be targeted at the sites of greatest pain. It also allows guided diagnostic and therapeutic intervention, such as percutaneous drainage (25,39,40). However, there are no US characteristic signs for identification of AVN.

Its main value is to identify or exclude other lesions mainly osteomyelitis, septic arthritis, and to some extent post-traumatic sequelae which are the main differential diagnosis in acute bone crisis. In addition, it is a useful means for guided aspiration.

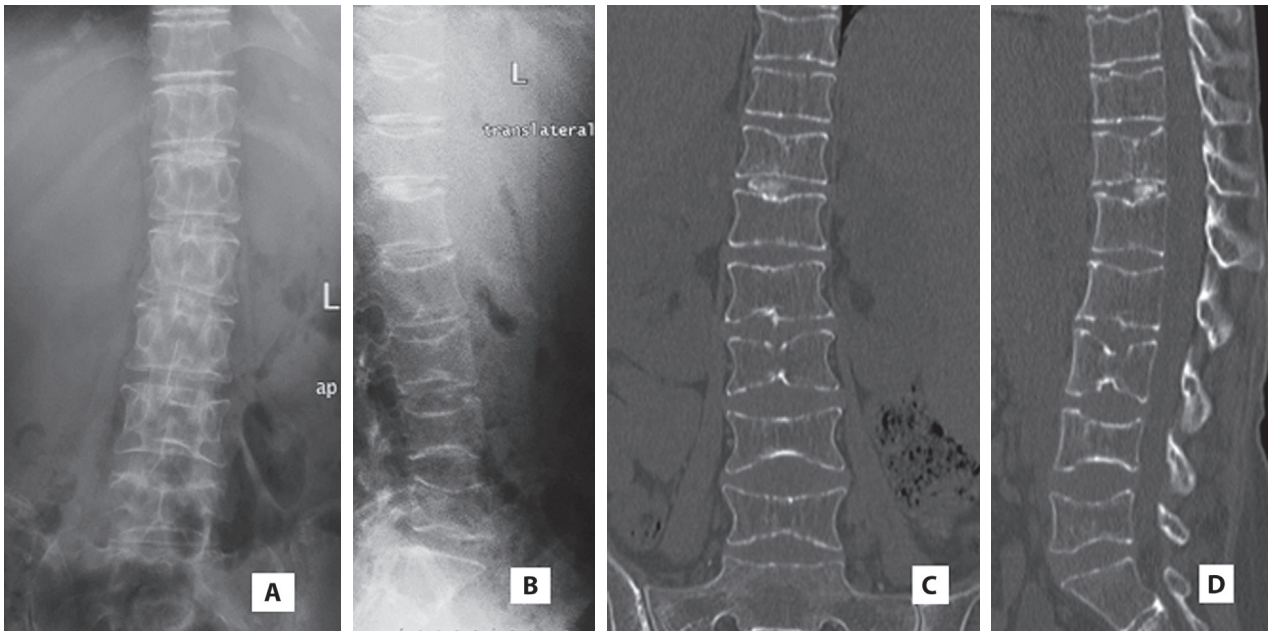

Figure 19. Plain x-ray lumbar spines AP and lateral views (A and B), coronal and sagittal reconstructed CT images (C and D) showing marked osteopenia of the lumbar and lower dorsal vertebrae with prominent linear trabeculation 2ry to bone marrow hyperplasia central endplate compression in almost all the lumbar vertebral bodies resulting in H -shaped vertebral bodies with step like the central depression of the articular end plates more identified at L3 Intervertebral disc, calcification noted within 12-L1 disc. No definite features of vertebral osteomyelitis. No paravertebral soft tissue lesions were identified, CT images are more informative and more clearing up the nature and extent of the AVN of the articular end plates of lumbar vertebrae than plain radiography (as accurate as MRI).

e. Isotope study

For the cases of AVN, it is very sensitive in the detection of abnormality, especially in early (acute) cases which appear as areas of low intake but unfortunately have relatively low specificity, still can be used to diagnose associated osteomyelitis and in follow-up evaluation.

The appearances of infarction at scintigraphy with 99mTc methylene diphosphonate (MDP) vary with time and may be difficult to interpret if the duration of symptoms is not known at the time of scanning. In the first few days after infarction, decreased or normal radiotracer uptake is seen (25). Subsequently, revascularization, primarily from periosteal vessels, produces increased uptake that extends with remodeling. The appearance of old bone infarcts depends on whether an adequate blood supply returns to the affected area. In areas of adequate revascularization, the scintigraphic appearance may return to normal after a few months; in contrast, areas of avascular bone are seen as photogenic foci.

Knowledge of the varied scintigraphic appearances of infarction is important, particularly if scintigraphy is performed because of clinical indications of acute osteomyelitis. Combined isotope bone scans and labeled white cell scans may be helpful, with triple-phase bone scans showing increased activity in all 3 phases. Labeled white cell scans can show increased uptake in infection with reduced uptake in areas of infarction, but the diffuse marrow abnormality present can hinder interpretation (25,41-44).

The combined use of scintigraphy and ultrasonography (US) can also be helpful in differentiating osteomyelitis from bone infarction. The scintigraphic studies are useful in locating all areas of suspected osteomyelitis while the role of the US is to confirm the presence of a subperiosteal fluid collection and to guide aspiration with analysis of the aspirate distinct between a hematoma and an abscess (25).

Detailed examples of the radiological manifestations of the common sites complicated with AVN and osteonecrosis in SCD are illustrated below (head of the femur, shoulder joint, vertebrae, and others).

Contrary to the AVN that can occur in other diseases, AVN in SCD can present diffusely, and lesions seen on MRI usually appear bigger. In most cases of avascular necrosis in SCD, the initial radiographic images can have a normal appearance, and the first evidence of this complication can be seen on MRI.

Osteonecrosis involving epiphyseal regions of long bones is generally termed avascular necrosis. The most common locations involved are the heads of the femur and humerus. AVN may be of gradual onset and silent or run a more acute course with severe pain and limping. The infarcted portions of the medullary bone eventually evolve into regions of reactive sclerosis and new bone formation (25,45-49).

a. AVN of the hip (UFCE)

Two broad patterns of involvement of the hip region were discernible according to the age of onset. Involvement of the immature femoral head epiphysis resulted in a flattened femoral head, epiphysis-metaphyseal overlap, a wide femoral neck, and a mushroom deformity of the mature femoral head. In these lesions, the articular surface and joint space were generally well preserved, and little or no disability resulted (Figure 17) (25).

In adult patients, involvement of the mature femoral head was typically segmental, most commonly anterosuperior, and with continued weight, bearing resulted in the collapse of the head and disruption of the articular surface. These lesions caused pain, limitation of movement, and common changes to osteoarthrosis. The radiological change occurred, by definition, in the femoral head of all hips, and occurred in the acetabulum in 72% of hips, femoral head migration occurred in 9% of hips, and periosteal new bone formation in 32% of hips (47,49) (Figures 1,2,6-9,11,13,14,16).

Multiple small-diameter drilling decompressions can be performed as a line of treatment for the AVN and followed up regularly for assessment of the progression and healing of the lesions by pre and postoperative X-ray and or MRI examinations (Figure 17) (50). Advanced cases of AVN femoral heads necessitate hip replacement as a definite line of management (Figure 14) (51).

b. AVN affecting the shoulder joint

It is as frequent or slightly less than the frequency of hip involvement and the classifications used in hip joint quantification can be applied to the shoulder, the degree of disability of the shoulder can be severe and may require shoulder replacement in some patients (Figures 3, 5,10,12,15) (11,29,52,53).

c. AVN involving the long bones and knee regions

Osteonecrosis of long bones and knee; Both in children and in adults the long bones are the more common sites of bone infarction and medullary bone infarcts are far more common than osteomyelitis in patients with sickle cell disease (25,34), metaphyseal or diaphyseal osteonecrosis leads to a characteristic appearance of irregular linear serpiginous areas of intramedullary signal intensity changes mainly edema followed by sclerosis prior to or 2ry to bone infarct (Figures 2,4). Later, intramedullary lucencies and sclerosis become evident with a patchy distribution. If the cortical bone is also infarcted, subperiosteal new bone may form either through incorporation into existing cortical bone (thickening of the cortex) or through layered deposits along the inner surface of the cortex (25,34).

AVN of the knee regions are relatively common and initial plain radiographs, in early-onset are usually negative but the lesions are more/mainly identified by MRI examinations with the serpiginous hyperintensity in T2 as well as mosaic hypo and hyperintensities in both T1 and T2 sequences according to the chronicity and severity of the involvement (Figure 18), while bone scintigraphy may show initial photopenia (low intake), but as the bone revascularizes uptake may return to normal or even be increased. This makes interpretation of the radioisotope imaging difficult as the relevance of the imaging findings is related to the length of time since the infarction evolve, while the changes in plain radiographs appear relatively later and are usually heterogeneous patchy sclerotic and lytic areas with less frequently periosteal reaction (Figure 20) (29,52-54).

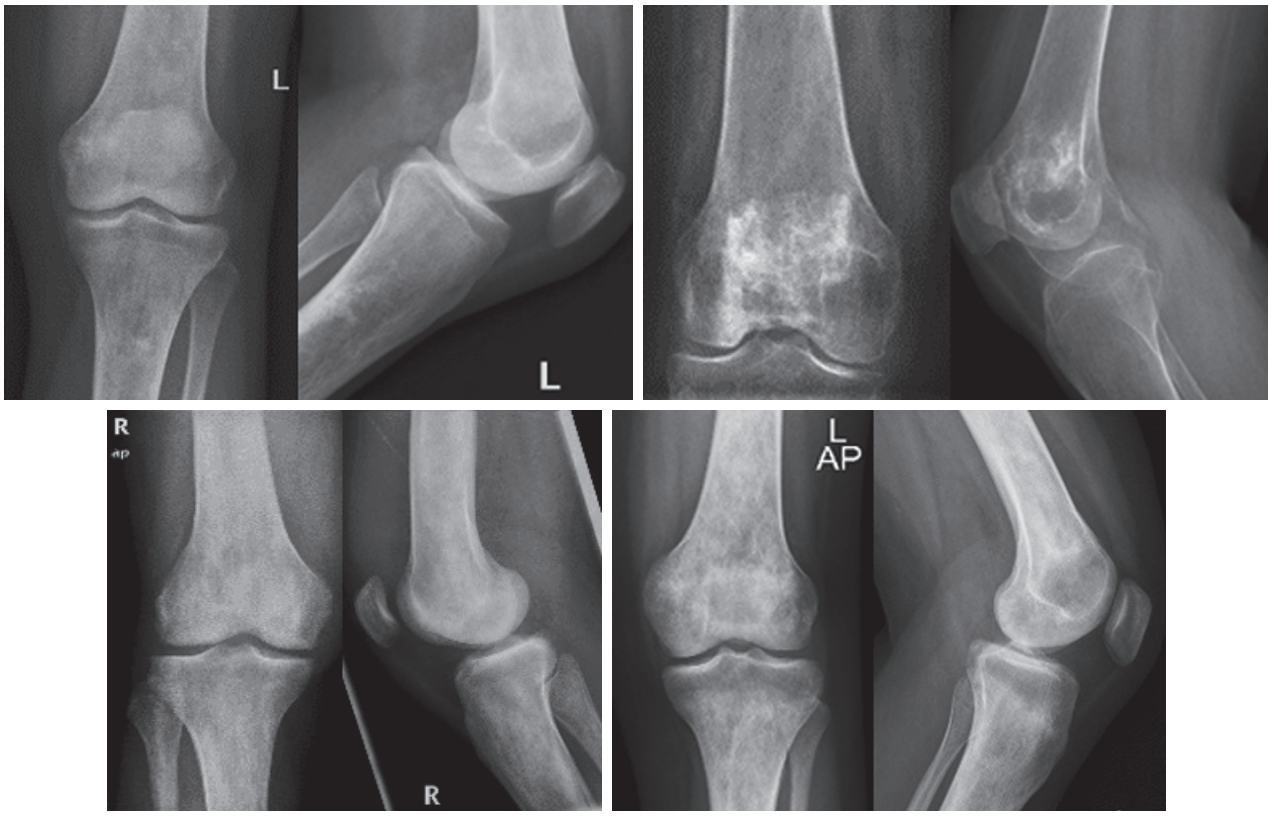

Figure 20. Plain X-ray knee region (AP and lateral views) of four different patients with SCD showed variable degrees of irregular sclerotic and lytic areas involving epiphysis, metaphysis, and diaphysis of lower femora and upper tibiae 2ry to avascular bone necrotic changes with no obvious articular surfaces involvement, no bone collapse or obvious periosteal reaction.

d. AVN vertebrae

Vertebral endplate infarction causes cortical thinning and softening of the bone, the intervertebral disks can then compress the weakened endplates, giving the vertebral bodies a biconcave or H-shaped appearance, which is the cardinal manifestation of vertebral endplate infarction in SCD (25,29,46,54). Central endplate depression can be differentiated from marrow hyperplasia and other causes of end plate depressions by its specific and characteristic step-like appearance (34). As a result of this endplate depression, vertebrae that are adjacent to the H-shaped vertebrae may exhibit lengthening to compensate for the change in shape and to support the spinal column. This deformity should be differentiated from the smooth concavity of the vertebral endplates at multiple levels which occurred from bone softening 2ry to bone marrow hyperplasia (fish vertebra). Bone marrow expansion secondary to increased production of red cells also contributes to thinning of cortical bone and osteopenia, this weakening of the bone can result in vertebral body compression or collapse with resultant kyphosis (31).

In cases of associated discitis and vertebral body osteomyelitis MR scanning is the preferred method of assessment (25,46) which showed high signal on T2 weighted images in the affected disc or vertebral body and in T1 sequences osteomyelitis is of low signal intensity (although areas of red marrow will also be of low signal intensity) post-contrast enhancement of the abnormal areas tend to be more diffuse in infection than in infarction, rim enhancement may also be seen but is not specific as it is also seen in bone infarction (13). Soft tissue enhancement is again not specific for infection and can be seen in both. Plain X-ray can identify the H-shaped vertebrae and the step central end plate depressions (Figures 19,21) as well

as the vertebral collapse (Figure 22) but CT reconstructed images in the bone window (Figure 19,23) and MRI sagittal and coronal sequences showed more precise diagnostic accuracy (Figure 23) especially in initial diagnosis and provide more information about the other findings like osteoporosis, bone marrow hyperplasia and hemosiderin/iron deposition within the vertebral bodies as well as the associated other complications like discitis/osteomyelitis of the vertebrae (Figure 22).

e. Ribs and pelvis

Other bones, such as the pelvis and ribs, may become markedly sclerotic because of medullary infarction as dystrophic medullary calcification occurs and new bone is laid down on infarcted bone (Figure 24). Infarction of the ribs in patients with sickle cell disease (Figure 25) may contribute to painful chest crises with resultant hypoventilation and pulmonary infiltrates (Figure 26) (34).

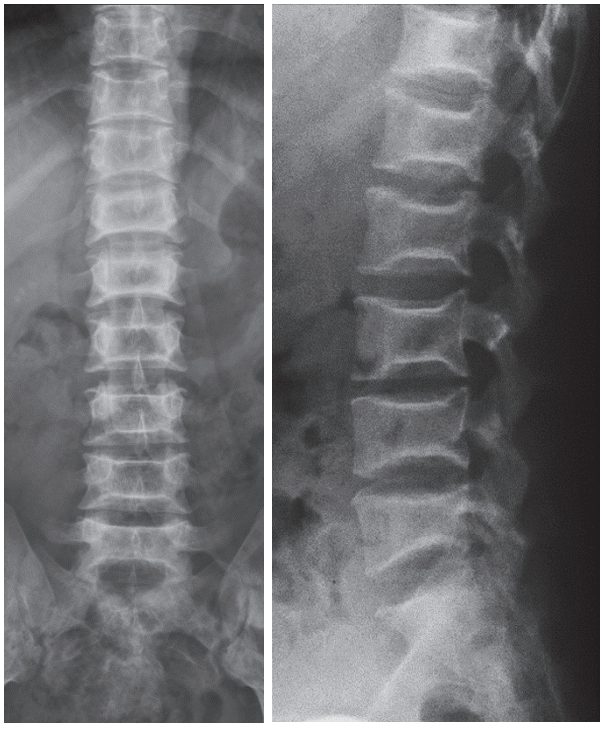

Figure 21. AP and Lateral views of lumbar vertebrae for a patient with SCD demonstrating the typical articular end plate AVN with step-like depression of the central portion of most lumbar and lower dorsal vertebral articular end plates and 2ry H shaped vertebral bodies which is characteristic for AVN of articular end plates.

f. Dactylitis "hand–foot" syndrome

Infarction of small tubular bones of the hands and feet in children causes dactylitis, also referred to as hand-foot syndrome. This is the most familiar site between in children between 6 months and 6 years of age because their red marrow is abundant in the small bones. Dactylitis is rare in children older than 6 years because of the regression of red marrow in these areas.

This syndrome occurs in half of the children with sickle cell anemia. The child will present with tender and swollen hands or feet and a fever. On radiographs, there is patchy lucencies with periosteal reaction early in the process followed by sclerosis with possible bone destruction and deformity over time. MRI will show osseous and soft-tissue edema and contrast enhancement, along with periosteal reaction. In more severe cases, bone destruction and resultant deformity may be seen (55 -57).

In summary

Based on the previous review, we suggest a key algorithm to be followed in the radiological evaluation and or follow up of patients with AVN or suspected AVN (Table 5).

Conflicts of Interest: Each author declares that he has no commercial associations (e.g., consultancies, stock ownership, equity interest, patent/licensing arrangement etc.) that might pose a conflict of interest in connection with the submitted article.

Author Contributions: EMAB conceived the study, has the responsibility for the integrity and accuracy of the imaging data, constructed the tables and figures, and edited the first draft. MY, and NJA reviewed and edited the manuscript. All the authors approved the final version of the submitted manuscript.

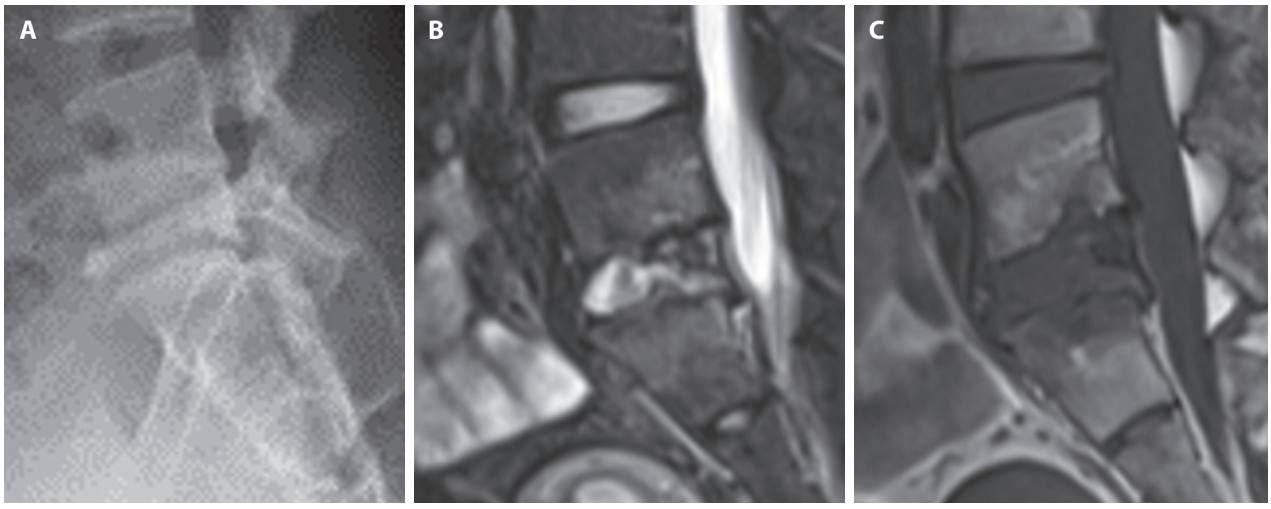

Figure 22. Plain X-ray lumbosacral region lateral view (A), MRI sagittal T2 with fat sat (B) and Sagittal T1 without fat sat (C) for a patient with SCD demonstrating old subtotal destruction and collapse of the body of L5 vertebra (A) later follow up with MRI showing the L4-5 and L5-S1 intervertebral discs appears now as a single disc space between the L4 and S1 vertebrae evidence of residual bone marrow edema and fatty infiltration within L4 and S1 vertebrae and in the residual part of L5 vertebra with minimal fluid in the anterior part of the wide L4-S1 intervertebral disc likely effects of chronic discitis together with central depression within the inferior end plate L4 and superior end plate S1 due to AVN of the end plates, no epidural or paravertebral fluid collections or abscess formation is detected.

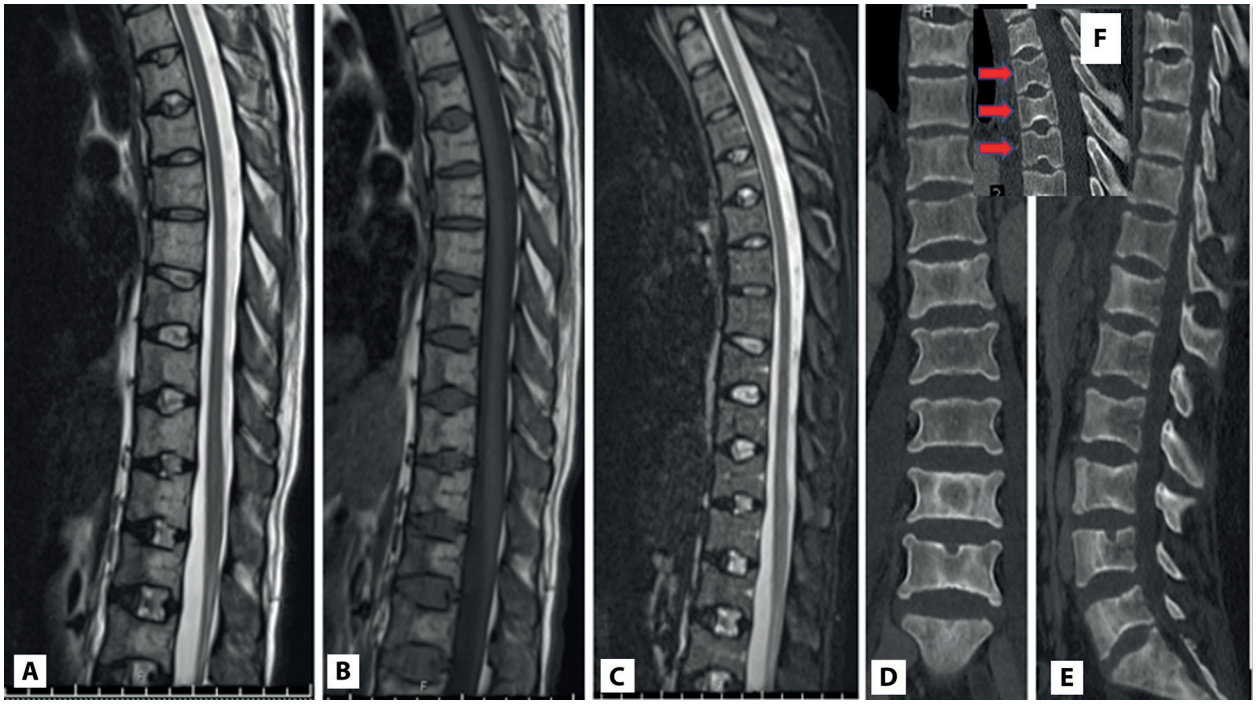

Figure 23. Dorsolumbar vertebrae A T2, B T1 and C T2stir sequences demonstrating the H-shaped vertebrae 2ry to AVN of the articular end plates of lower dorsal and upper lumbar vertebrae with central step-like depression of the articular end plates (typical for AVN) D and E are coronal and sagittal CT reconstructed images for another patient with H shape vertebrae and F focused sagittal CT reconstruction demonstrating typical H shaped vertebrae).

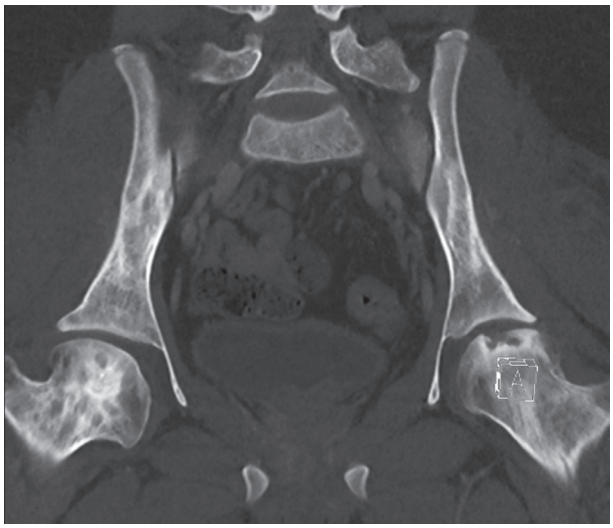

Figure 24. A reconstructed coronal CT scan for pelvis and hips revealed patchy sclerosis of the pelvic bone and upper femora with necrosis of the left femoral head (Grade III Ficat stage IVa Steinberg) caused by medullary infarction and dystrophic calcification.

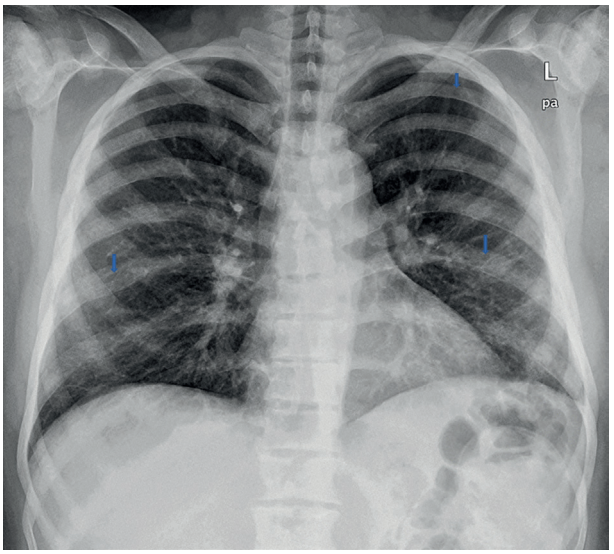

Figure 25. Multiple rib infarctions. Posteroanterior chest radiograph demonstrates dense sclerosis of the rib cage with relative expansion effects of bone marrow hyperplasia 2ry to SCD, with areas of lucency (arrows) in multiple ribs representing focal osteonecrosis.

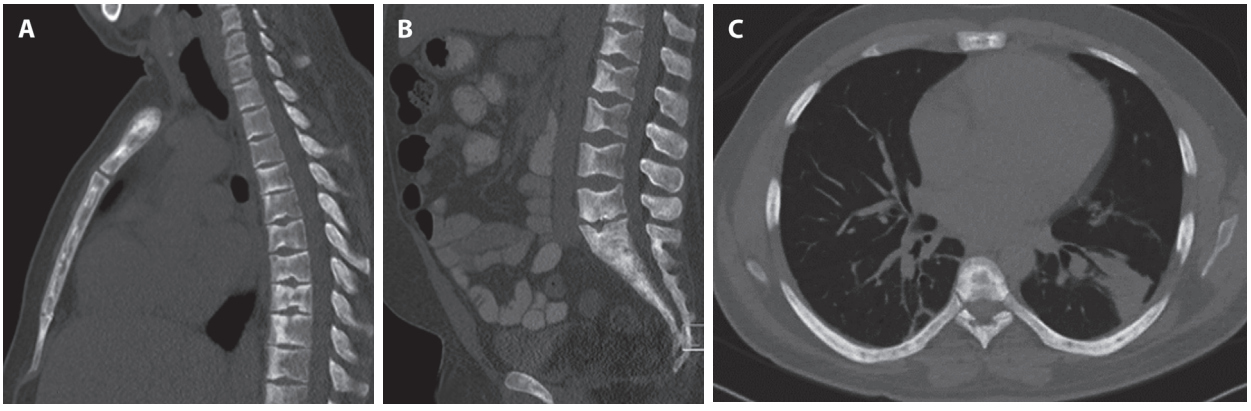

Figure 26. CT Chest and abdomen sagittal reconstructed images bone window (A and B) and lower chest axial cut lung window (C) for a patient with SCD revealed: Patchy sclerotic and small lytic changes within the sternum and ribs while dorsal and lumbosacral vertebrae showed, in addition, multiple articular end plates depressions with variable patchy sclerosis and prominent 1ry bone trabeculae 2ry to mixed bone marrow infarcts and hyperplasia of hemopoietic system, Note pneumonic patch at left posterior basal segment.

Table 5. Algorithm for imaging evaluation of AVN.

1. Patients known to have SCD and AVN in certain location followed up with no new complaint or further complication: a. In early low grade AVN no rule for plain radiography, no need for CT, follow up with MRI. b. In late and high grades of AVN: plain radiographs are enough + or - MRI/CT if significant changes from previous examinations.
2. Patients known to have SCD and AVN in certain locations with relative clinical excerption of their AVN location. a. In early low grade AVN Plain radiograph may have limited rule and MRI or CT still advised. b. In late and high grades of AVN: plain radiographs may be enough + or - MRI/CT if significant changes from previous examinations.
3. Patients Known to have SCD with previous history of AVN but having a new location for bone crisis. a-Isotope bone scan and or MRI + or -US if clinically indicated grossly no rule for plain radiographs.
4. Patient known to have SCD with no previous history of AVN presenting with acute bone crisis. a. Isotope bone scan and or MRI + or -US if clinically indicated grossly no rule for plain radiographs.
5. Patients not known to have SCD are presented with acute bone crisis. a. exclude SCD by lab investigation. b. US examination for joint or bone involved. c. plain X ray for area of interest if US is grossly negative or if fracture is suggested by US. d. MRI or CT if plain X ray is negative.

References

1. Yu T, Campbell T, Ciuffetelli I, et al. Symptomatic Avascular Necrosis: An Understudied Risk Factor for Acute Care Utilization by Patients with SCD. South Med J. 2016 ;109(9):519-24. doi: 10.14423/SMJ.0000000000000512.
2. Vijaya Kosaraju, Alok Harwani, Sasan Partovi, et al. Imaging of musculoskeletal manifestations in sickle cell disease patients. AJR, 2017; 90(1073): 20160130. doi: 10.1259 /bjr.20160130.
3. Martí-Carvajal AJ, Solà I, Agreda-Pérez LH. Treatment for avascular necrosis of bone in people with sickle cell disease. Cochrane Database Syst Rev. 2019, 5;12(12):CD004344. doi: 10.1002/ 14651858.CD004344.pub7.
4. Akinyoola AL, Adediran IA, Asaleye CM. Avascular necrosis of the femoral head in sickle cell disease in Nigeria: a retrospective study. Niger Postgrad Med J. 2007;14(3):217–20. PMID: 17767206.
5. Akinyoola AL, Adediran IA, Asaleye CM,et al. Risk factors for osteonecrosis of the femoral head in patients with sickle cell disease. Int Orthop. 2009,33(4):923-6. doi: 10.1007 /s00264-008-0584-1.
6. Milner PF, Kraus AP, Sebes JI, et al. Sickle cell disease as a cause of osteonecrosis of the femoral head. N Engl J Med. 1991;325(21):1476–81. doi: 10.1056/NEJM199111 213252104.
7. Hernigou P, Habibi A, Bachir D, Galacteros F. The natural history of asymptomatic osteonecrosis of the femoral head in adults with sickle cell disease. Bone Joint Surg Am. 2006;88(12):2565–2572. doi: 10.2106/JBJS.E.01455.
8. Almeida A, Roberts I. Bone involvement in sickle cell disease. Br J Haematology. 2005 May;129(4):482-90. doi: 10.1111 /j.1365-2141.2005.05476. x.
9. Vaishya R, Agarwal AK, Edomwonyi EO, et al. Musculoskeletal Manifestations of Sickle Cell Disease: A Review. Cureus. 2015;20;7(10):e358. doi:10.7759/cureus.358.
10. Ware HE, Brooks AP, Toye R, et al. Sickle cell disease and silent avascular necrosis of the hip. J Bone Joint Surg Br. 1991; 73:947–949. doi:10.1302/0301-620X.73B6.1955442.
11. Babhulkar SS, Pande KC, Babhulkar SS. Clinical review of osteonecrosis of humeral head in sickle cell haemoglobinopathy (Study of 258 shoulders). J Shoulder Elbow Surg. 1996; 5: S63. doi:org/10.1016/s1058-2746(96)80300-4.
12. Claster S, Vichinsky EP. Managing sickle cell disease. BMJ. 2003; 327: 1151–5. doi: https://doi.org/10.1136 /bmj.327.7424.1151.
13. Lonergan GJ, Cline DB, Abbondanzo SL. Sickle cell anemia. Radiographics 2001; 21:971-94. doi: 10.1148/radiographics. 21.4. g01jl23971.
14. Hagar RW, Vichinsky EP. Major changes in sickle cell disease. Adv Pediatr. 2000; 47:249–72. PMID: 10959446.
15. Schmitt R, Kalb KH, Christopoulos G, et al. Osteonecrosis of the Upper Extremity: MRI-Based Zonal Patterns and Differential Diagnosis. Semin Musculoskelet Radiol. 2019 .23(5):523-33. doi: 10.1055/s-0039-1695719.
16. Naseer ZA, Bachabi M, Jones LC, et al. Osteonecrosis in Sickle Cell Disease. South Med J. 2016;109(9):525-30. doi: 10.14423/SMJ.0000000000000516.
17. Kopecky KK, Braunstein EM, Brandt KD, et al. Apparent avascular necrosis of the hip: appearance and spontaneous resolution of MR findings in renal allograft recipients. Radiology. 1991;179(2):523-7. doi: 10.1148/radiology.179.2.2014304.
18. Jawad MU, Haleem AA, Scully SP. In brief: Ficat classification: avascular necrosis of the femoral head. Clin Orthop Relat Res. 2012 ;470(9):2636-9. doi: 10.1007/s11999 -012-2416-2.

19. Mukisi-Mukaza M, Gomez-Brouchet A, Donkerwolcke M, et al. Histopathology of aseptic necrosis of the femoral head in sickle cell disease. Int Orthop. 2011 ;35(8):1145-50. doi: 10.1007/s00264-010-1121-6.
20. Bahebeck J, Atangana R, Techa A, et al. Relative rates and features of musculoskeletal complications in adult sicklers. Acta Orthop Belg. 2004; 70: 107–11. PMID: 15165010.
21. Ballas SK, Lieff S, Benjamin LJ, et al. Investigators, Comprehensive Sickle Cell Centers. Definitions of the phenotypic manifestations of sickle cell disease. Am J Hematol. 2010 ;85(1):6-13. doi: 10.1002/ajh.21550.
22. Mitchell DG, Rao VM, Dalinka MK, Spritzer CE, et al. Femoral head avascular necrosis: correlation of MR imaging, radiographic staging, radionuclide imaging, and clinical findings. Radiology. 1987;162(3):709-15. 26. doi: 10.1148 /radiology.162.3.3809484.
23. Yoon BH, Mont MA, Koo KH, et al. The 2019 Revised Version of Association Research Circulation Osseous Staging System of Osteonecrosis of the Femoral Head. J Arthroplasty. 2020 ;35(4):933-940. doi: 10.1016/j. arth.2019.11.029.
24. Steinberg ME, Hayken GD, Steinberg DR. A quantitative system for staging avascular necrosis. J Bone Joint Surg Br. 1995;77 (1): 34-41. PMID: 7822393.
25. Ejindu VC, Hine AL, Mashayekhi M, Shorvon PJ, et al. Musculoskeletal manifestations of sickle cell disease. Radiographics. 2007,27(4):1005-21. doi: 10.1148/rg.274065142.
26. Jawad MU, Haleem AA, Scully SP. In brief: Ficat classification: avascular necrosis of the femoral head. Clin. Orthop. Relat. Res. 2012;470 (9):2636-9.doi:10.1007/s11999 -012-2416-2.
27. Ficat RP, Arlet J. Necrosis of the femoral head. In: Hungerford DS, eds. Ischemia and necrosis of bone. Baltimore, Md: Williams & Wilkins, 1980; pp.171-182.
28. Beaule PE, Amstutz, HC: Management of Ficat stage III and IV osteonecrosis of the hip. J Amer Acad Orthop Surg. 2004; 12: 96-105. doi: 10.5435/00124635-200403000-00005.
29. Ejindu VC, Hine AL, Mashayekhi M, et al. Musculoskeletal manifestations of Sickle Cell Disease. RadioGraphics. 2007;27(4):1005-21. doi: 10.1148/rg.274065142.
30. Elalfy MS, Fadhli I, Mohammad S, et al. Avascular Necrosis of the Femoral Head in Sickle Cell Disease in Egypt and Oman: A Cross Sectional Study. Blood. 2018; 132 (Supplement 1): 4921. doi.org/10.1182/blood-2018-99-116683.
31. Ganguly A, Boswell W, Aniq H. Musculoskeletal manifestations of sickle cell anaemia: a pictorial review. Anemia. 2011;2011:794283. doi: 10.1155/2011/794283.
32. Keeley K, Buchanan GR. Acute infarction of long bones in children with sickle cell anemia. J Pediatr. 1982,101(2):170-5. doi: 10.1016/s0022-3476(82)80111-x.
33. Madani G, Papadopoulou AM, Holloway B, et al. The radiological manifestations of sickle cell disease. Clin Radiol. 2007;62(6):528-38. doi: 10.1016/j.crad.2007.01. 006..
34. Meier R, Kraus TM, Schaeffeler C, et al. Bone marrow oedema on MR imaging indicates ARCO stage 3 disease in patients with AVN of the femoral head. Eur Radiol. 2014;24(9):2271-8. doi: 10.1007/s00330-014-3216-8.
35. Barille MF, Wu JS, McMahon CJ. Femoral head avascular necrosis: a frequently missed incidental finding on multidetector CT. Clin Radiol. 2014 ;69(3):280-5. doi: 10.1016/j. crad. 2013.10.012.
36. Azzali E, Milanese G, Martella I, et al. Imaging of osteonecrosis of the femoral head. Acta Biomed. 2016 28;87 Suppl 3:6-12. PMID: 27467861.
37. Iqbal B, Currie G. Value of SPECT/CT in the diagnosis of avascular necrosis of the head of femur: A meta-analysis. Radiography (Lond). 2022 ;28(2):560-4. doi: 10.1016 / j.radi. 2021. 11.012.
38. Luk WH, Au-Yeung AW, Yang MK. Diagnostic value of SPECT versus SPECT/CT in femoral avascular necrosis: preliminary results. Nucl Med Commun. 2010 ;31(11):958-61. doi: 10.1097/MNM.0b013e32833e7732.
39. Sidhu PS, Rich PM. Sonographic detection and characterization of musculoskeletal and subcutaneous tissue abnormalities in sickle cell disease. Br J Radiol. 1999; 72:9 –17. doi: 10.1259/bjr.72.853.10341683
40. Booz MM, Hariharan V, Aradi AJ, et al. The value of ultrasound and aspiration in differentiating vaso-occlusive crisis and osteomyelitis in sickle cell disease patients. Clin Radiol 1999; 54:636 – 9. doi: 10.1016/s0009-9260(99)91081-4.
41. Palestro CJ, Love C, Tronco G, et al. Combined labeled leukocyte and technetium 99m sulfur colloid bone marrow imaging for diagnosing musculoskeletal infection. Radiographics 2006; 26:859 – 70. doi: 10.1148/rg.263055139.
42. Love C, Palestro CJ. Radionuclide imaging of infection. J Nucl Med Technol. 2004; 32:47–57. PMID: 15175400.
43. Palestro CJ, Love C. Radionuclide imaging of musculoskeletal infection. Braz Arch Biol Technol. 2007;50:15-27. doi: 10.1055/s-2008-1060336.
44. Palestro CJ, Roumanas P, Swyer AJ, et al. Diagnosis of musculoskeletal infection using combined In-111 labeled leukocyte and Tc-99m SC marrow imaging. Clin Nucl Med. 1992 ;17(4):269-73. doi: 10.1097/00003072-199204000-00001.
45. Resnick D. Hemoglobinopathies and other anemias. In: Resnick D, ed. Diagnosis of bone and joint disorders. 4th ed. Philadelphia, Pa: Saunders, 2002; 2146 –87. PMID: 2296457.
46. Malizos KN, Siafakas MS, Fotiadis DI, et al. An MRI-based semiautomated volumetric quantification of hip osteonecrosis. Skeletal Radiol. 2001; 30: 686–93.doi: 10.1007 / s002560100399.
47. Calder JD, Hine AL, Pearse MF, et al. The relationship between osteonecrosis of the proximal femur identified by MRI and lesions proven by histological examination. J Bone Joint Surg Br. 2008 ;90(2):154-8. doi: 10.1302/0301-620X.90B2.19593.
48. Lonergan GJ, Cline DB, Abbondanzo SL. Sickle cell anemia. Radiographics 2001; 21:971-94. doi: 10.1148/radio graphics.21.4.g01jl23971 .
49. Lee RE, Golding JS, Serjeant GR. The radiological features of avascular necrosis of the femoral head in homozygous

sickle cell disease. Clin Radiol. 1981 ;32(2):205-14. doi: 10.1016/ s0009-9260(81)80162-6.
50. Li J, Li ZL, Zhang H, et al. Long-term Outcome of Multiple Small-diameter Drilling Decompression Combined with Hip Arthroscopy versus Drilling Alone for Early Avascular Necrosis of the Femoral Head. Chin Med J (Engl). 2017; 130(12):1435-40. doi: 10.4103/ 0366-6999.207470.
51. Al-Otaibi ML, Waliullah S, Kumar V. Total Hip Replacement in Sickle Cell Disease Patients with Avascular Necrosis of Head of Femur: A Retrospective Observational Study. Indian J Orthop. 2021, 28;55(5):1225-31. doi: 10.1007 /s43465-021-00394-6.
52. Ombregt L, Bisschop P, ter Veer HJ. A system of orthopaedic medicine. Elsevier Health Sciences, 2003. ISBN: 0443073708, 9780443073700.
53. Murphey M, Foreman K, Klassen-Fischer M, et al. From the Radiologic Pathology Archives Imaging of Osteonecrosis: Radiologic-Pathologic Correlation. Radiographics. 2014;34(4):1003-28. doi: 10.1148/rg.344140019.
54. Yoon B, Mont M, Koo K, et al. The 2019 Revised Version of Association Research Circulation Osseous Staging System of Osteonecrosis of the Femoral Head. J Arthroplasty. 2020;35(4):933-40. doi: 10.1016/j.arth.2019.11.029 .
55. Babhulkar SS, Pande K, Babhulkar S. The hand-foot syndrome in sickle-cell haemoglobinopathy. J Bone Joint Surg Br. 1995;77(2):310-2. PMID: 7706355.
56. Kennedy DP, Hooker JD, Morris RW. Osseous Findings in Sickle Cell Disease. Applied Radiol. 2020; 49 (2) https://appliedradiology.com/communities/pediatric-imaging/osseous-findings-in-sickle-cell-disease
57. Resnick D, Kransdorf MJ. Hemoglobinopathies and Other Anemias. Bone and joint imaging: Philadelphia, PA: Elsevier BV; 2005. pp. 635–51.

Correspondence:
Received: 11 April 2023
Accepted: 11 May 2023
Elsaid Mohamed Aziz Bedair, MD
Professor and Senior Consultant, Radiology Department, AlKhor Hospital, HMC, Doha, Qatar
Phone: +974 66696894
E-mail: elsaid_bedair@hotmail.com, ebedair@hamad.qa